

**EFFECT OF LIGAMENT GEOMETRY ON THE STRESS AT BONE INSERTION
SITES**

by

Nithin Reddy Karna

B.E in Mechanical Engineering, Birla Institute of Science & Technology- Pilani, 2011

Submitted to the Graduate Faculty of
Swanson School of Engineering in partial fulfillment
of the requirements for the degree of
Master of Science in Mechanical Engineering

University of Pittsburgh

2016

UNIVERSITY OF PITTSBURGH
SWANSON SCHOOL OF ENGINEERING

This thesis was presented

by

Nithin Reddy Karna

It was defended on

July 27, 2016

and approved by

Mark C Miller, PhD, Associate Professor, Department of Mechanical Engineering
and Materials Science

Qing Ming Wang, PhD, Professor, Department of Mechanical Engineering and Materials
Science

Thesis Advisor: Patrick Smolinski, PhD, Associate Professor, Department of Mechanical
Engineering and Materials Science

Copyright © by Nithin Reddy Karna

2016

EFFECT OF LIGAMENT GEOMETRY ON THE STRESS AT THE BONE INSERTION SITES

Nithin Reddy Karna, M.S.

University of Pittsburgh, 2016

Objective: The focus of this study is to identify the significance of the ligament shape at the bone insertion sites and how it affects the stresses at the locations.

A ligament is a dense bundle of connective tissues made up of fibers that connects one bone and another bone to control joint motion and transfer load. This study was focused on stress at the bone insertion site where the ligament attaches to the bone. The present study was done to determine the importance of using nonlinear elastic properties and non-uniform geometry of the ligament when analyzed under a tensile load. A 2D axis-symmetry model was considered for the ligament and the bone was chosen to be a rigid material body and a non-linear static analysis was performed to assess the stress at the bone- ligament interface.

Results: The von Mises stresses at the insertion sites were predicted. Effect of different ligament geometry shapes was studied by comparing the stress results.

Clinical or Engineering Relevance: The results allow a better understanding of the shape of ligament morphology due to the load.

TABLE OF CONTENTS

PREFACE.....	XVI
1.0 INTRODUCTION.....	1
1.1 MOTIVATION	1
1.2 OBJECTIVE	2
2.0 STRUCTURE AND FUNCTION OF LIGAMENTS	3
2.1 LIGAMENT INSERTION.....	4
3.0 BACKGROUND	8
4.0 MATERIAL PROPERTIES OF LIGAMENTS	10
4.1 MATERIAL MODELS.....	11
5.0 FINITE ELEMENT ANALYSIS.....	15
5.1 CONSTITUTIVE MODEL OF LIGAMENTS.....	15
6.0 APPROACH & ANALYSIS.....	18
6.1 BOUNDARY AND LOADING CONDITIONS.....	18
6.2 GEOMETRY OF LIGAMENT	19
6.3 FINITE ELEMENT MESHING	23
7.0 RESULTS AND DISCUSSION	26
7.1 EFFECT OF VARYING DIAMETER.....	26
7.2 EFFECT OF VARIABLE EDGE LENGTH	34

7.3	EFFECT OF VARYING FILLET RADIUS.....	40
7.4	EFFECT OF VARYING ANGLE.....	48
7.5	EFFECT OF VARIABLE MINOR RADIUS	55
7.6	DISCUSSION.....	61
8.0	CONCLUSION.....	65
9.0	LIMITATIONS	66
APPENDIX A		67
	MAXIMUM STRAIN VALUES CALCULATED	67
APPENDIX B		70
	B.A: CASE II: EFFECT OF VARYING EDGE LENGTH	70
	B.B: CASE III: EFFECT OF VARYING FILLET RADIUS	75
	B.C: CASE IV: EFFECT OF VARYING ANGLE	80
	B.D: CASE V: EFFECT OF VARYING MINOR RADIUS	86
BIBLIOGRAPHY		92

LIST OF TABLES

Table 1: Maximum stress values and location for case I (Element size 0.09).....	31
Table 2: Maximum stress value and locations for case II.....	38
Table 3: Maximum stress values and location for case III mesh size h size 0.09	45
Table 4: Maximum stress values and location for case IV (Element size 0.09).....	52
Table 5: Maximum stress locations for case V (mesh size 0.09).....	59
Table 6 : Effect of geometry on von Mises stress for the same edge length	64
Table 7 : Maximum strain values for case I (variable cylinder diameter)	67
Table 8: Maximum strain values for case II	68
Table 9: Maximum strain values for case III (fillet radius)	68
Table 10: Maximum strain values for case IV (fillet angle).....	68
Table 11: Maximum strain values for case V (minor radius)	69
Table 12: Results for the case II with mesh size 0.07.....	70
Table 13: Results for the case II with mesh size 0.25.....	71
Table 14: Results for the case III with mesh size 0.07	75
Table 15: Results for the case III with mesh size 0.25	76
Table 16: Results for the case IV with mesh size 0.25	81
Table 17: Results for the case IV with mesh size 0.07	81
Table 18: Results for the case V with mesh size 0.25	87

Table 19: Results for the case V with mesh size 0.07 87

LIST OF FIGURES

Figure 1: Indirect Ligament Insertion (Freddie H. Fu et al., 2008)	5
Figure 2: Direct Ligament Insertion (Freddie H. Fu et al., 2008).....	6
Figure 3: Shape of ligament where it attached the bone (Kevin D Plancher et.,al 2005).....	7
Figure 4: Force - Deformation curve for ligaments (Martin 1998)	11
Figure 5: Strain energy vs strain for cubic polynomial model (W_2) and Pioletti model (W_1).....	17
Figure 6: Boundary and load conditions on the ligament	19
Figure 7: Ligament geometry for Case I.....	20
Figure 8:Ligament geometry for Case II	20
Figure 9: Ligament geometry for Case III	21
Figure 10: Ligament geometry for Case IV	22
Figure 11: Ligament geometry for Case V	22
Figure 12: Meshed model of the ligament for Case I	24
Figure 13: Meshed model of the ligament for Case II.....	24
Figure 14: Meshed model of the ligament for Case III.....	24
Figure 15: Meshed model of the ligament for Case IV	24
Figure 16: Meshed model of the ligament for Case V.....	25
Figure 17: Case I with diameter of 10 mm	27

Figure 18: Maximum displacement vs diameter.....	28
Figure 19: Maximum von Mises stress vs diameter	28
Figure 20: Normal axial stress vs diameter.....	29
Figure 21: Normal radial stress vs diameter	29
Figure 22: Maximum shear stress vs diameter	30
Figure 23: von Mises stress (MPa) plot for Case I (Diameter 10mm).....	30
Figure 24: Normal axial stress (MPa) plot for Case I (Diameter 10mm)	30
Figure 25: Normal radial stress (MPa) plot for Case I (Diameter 10mm).....	31
Figure 26: Shear stress (MPa) plot for Case I (Diameter 10mm).....	31
Figure 27: Mesh sensitivity for von Mises stress	32
Figure 28: Mesh sensitivity for normal axial stress	32
Figure 29: Mesh sensitivity for normal radial stress.....	33
Figure 30: Mesh sensitivity for shear stress.....	33
Figure 31: Case II for edge length 6mm	34
Figure 32: Case II for edge length 10mm	34
Figure 33: Maximum displacement vs edge length	35
Figure 34: von Mises stress vs edge length	35
Figure 35: normal axial stress vs edge length.....	36
Figure 36: normal radial stress vs edge length.....	36
Figure 37: maximum shear stress vs edge length	36
Figure 38: von Mises stress (MPa) plot (Edge length 7mm).....	37
Figure 39: Normal axial stress (MPa) plot (Edge length 7mm).....	37
Figure 40: Normal radial stress (MPa) plot (Edge length 7mm)	37

Figure 41: Shear stress (MPa) plot (Edge length 7mm)	37
Figure 42: Mesh sensitivity for von Mises stress	39
Figure 43: Mesh sensitivity for normal axial stress	39
Figure 44: Mesh sensitivity for normal radial stress.....	39
Figure 45: Mesh sensitivity for shear stress.....	40
Figure 46: Case III with fillet radius 1mm.....	40
Figure 47: Case III with fillet radius 5mm.....	41
Figure 48: Maximum displacement vs fillet radius	41
Figure 49: von Mises stress vs fillet radius.....	41
Figure 50: Normal axial stress vs fillet radius	42
Figure 51: Normal radial stress vs fillet radius	42
Figure 52: Shear stress vs fillet radius	43
Figure 53: von Mises stress (MPa) plot for a fillet radius of 4mm.....	43
Figure 54: Normal axial stress (MPa) plot for a fillet radius of 4mm	43
Figure 55: Normal radial stress (MPa) plot for a fillet radius of 4mm	44
Figure 56: Shear stress (MPa) plot for a fillet radius of 4mm	44
Figure 57: Mesh sensitivity for von Mises stress	46
Figure 58: Mesh sensitivity for normal axial stress	46
Figure 59: Mesh sensitivity for normal radial stress.....	47
Figure 60: Mesh sensitivity for shear stress.....	47
Figure 61: Case IV with angle 30 degrees	48
Figure 62: Case IV with angle 60 degrees	48
Figure 63: Maximum displacement vs angle	49

Figure 64: von Mises stress vs angle	49
Figure 65: Normal axial stress vs angle.....	50
Figure 66: Normal radial stress vs angle.....	50
Figure 67: Shear stress vs angle.....	50
Figure 68: von Mises stress (MPa) plot for case IV (angle 45 deg.)	51
Figure 69: Normal radial stress (MPa) plot for case IV (angle 45 deg.)	51
Figure 70: Normal radial stress (MPa) plot for case IV (angle 45 deg.)	51
Figure 71: Shear stress (MPa) plot for case IV (angle 45 deg.).....	52
Figure 72: Mesh sensitivity for von Mises stress	53
Figure 73: Mesh sensitivity for normal axial stress	53
Figure 74: Mesh sensitivity for normal radial stress.....	54
Figure 75: Mesh sensitivity for shear stress.....	54
Figure 76: Case V with minor radius of 6mm	55
Figure 77: Case V with minor radius of 9mm	55
Figure 78: Displacement vs minor radius	56
Figure 79: von Mises stress vs minor radius.....	56
Figure 80: Normal axial stress vs minor radius	57
Figure 81: Normal radial stress vs minor radius.....	57
Figure 82: Shear stress vs minor radius	57
Figure 83: von Mises stress (MPa) plot for minor radius 8mm.....	58
Figure 84: Normal axial stress (MPa) plot for minor radius 8mm	58
Figure 85: Normal radial stress (MPa) plot for minor radius 8mm	58
Figure 86: Shear stress (MPa) plot for minor radius 8mm	59

Figure 87: Mesh sensitivity for von Mises stress	60
Figure 88: Mesh sensitivity for normal axial stress	60
Figure 89: Mesh sensitivity for normal radial stress.....	61
Figure 90: Mesh sensitivity for shear stress.....	61
Figure 91: Displacement (mm) plot for mesh size 0.09.....	72
Figure 92: Equivalent stress (MPa) plot for mesh size 0.09.....	72
Figure 93: Normal axial stress (MPa) plot for mesh size 0.09	72
Figure 94: Normal radial stress (MPa) plot for mesh size 0.09	72
Figure 95: Displacement (mm) plot for mesh size 0.07.....	73
Figure 96: Normal axial stress (MPa) plot for mesh size 0.07	73
Figure 97: Normal radial stress (MPa) plot for mesh size 0.07	73
Figure 98: Displacement (mm) for mesh size 0.25.....	74
Figure 99: Equivalent stress (MPa) plot for mesh size 0.25.....	74
Figure 100: Normal axial stress (MPa) plot for mesh size 0.25	74
Figure 101: Normal radial stress (MPa) plot for mesh size 0.25	74
Figure 102 Displacement (mm) plot for mesh size 0.09.....	77
Figure 103: Equivalent stress (MPa) plot for mesh size 0.09.....	77
Figure 104: Normal axial stress (MPa) plot for mesh size 0.09	77
Figure 105: Normal radial stress (MPa) plot for mesh size 0.09	77
Figure 106: Displacement (mm) plot for mesh size 0.07.....	78
Figure 107: Equivalent stress (MPa) plot for mesh size 0.07	78
Figure 108: Normal axial stress (MPa) plot for mesh size 0.07	78
Figure 109: Normal radial stress (MPa) plot for mesh size 0.07	78

Figure 110: Displacement (mm) plot for mesh size 0.25.....	79
Figure 111: Equivalent stress (MPa) plot for mesh size 0.25	79
Figure 112: Normal axial stress (MPa) plot for mesh size 0.25	80
Figure 113: Normal radial stress (MPa) plot for mesh size 0.25	80
Figure 114: Displacement (mm) plot for mesh size 0.09.....	82
Figure 115: Equivalent stress (MPa) plot for mesh size 0.09.....	82
Figure 116: Normal axial stress (MPa) plot for mesh size 0.09	82
Figure 117: Normal radial stress (MPa) plot for mesh size 0.09.....	83
Figure 118: Displacement (mm) plot for mesh size 0.25.....	83
Figure 119: Equivalent stress (MPa) plot for mesh size 0.25	83
Figure 120: Normal axial stress (MPa) plot for mesh size 0.25	84
Figure 121: Normal radial stress (MPa) plot for mesh size 0.25	84
Figure 122: Displacement (mm) plot for mesh size 0.07.....	85
Figure 123: Equivalent stress (MPa) plot for mesh size 0.07.....	85
Figure 124: Normal radial stress (MPa) plot for mesh size 0.07	86
Figure 125: Normal radial stress (MPa) plot for mesh size 0.07.....	86
Figure 126 : Displacement (mm) plot for mesh size 0.09.....	88
Figure 127: Equivalent stress (MPa) plot for mesh size 0.09.....	88
Figure 128: Normal axial stress (MPa) plot for mesh size 0.09	88
Figure 129: Normal radial stress (MPa) plot for mesh size 0.09	89
Figure 130: Displacement (mm) plot for mesh size 0.25.....	89
Figure 131: Equivalent stress (MPa) plot for mesh size 0.25	89
Figure 132: Normal axial stress (MPa) plot for mesh size 0.25	90

Figure 133: Normal radial stress (MPa) plot for mesh size 0.25	90
Figure 134: Displacement (mm) plot for mesh size 0.07.....	90
Figure 135: Equivalent stress (MPa) for mesh size 0.07	91
Figure 136: Normal axial stress (MPa) plot for mesh size 0.07	91
Figure 137: Normal radial stress (MPa) plot for mesh size 0.07	91

PREFACE

I would like to start by thanking Dr. Patrick Smolinski for accepting to be my research advisor. I have always looked up to him and have learnt a lot from him and his work within the short duration of my Master's degree program. I would also like to thank the University of Pittsburgh for providing me with excellent coursework and research facilities for my research work. I want to extend my gratitude to all the faculty and staff members of the Department of Mechanical Engineering and Material Science for guiding and helping me during this journey. Also my special thanks to Dr. Mark C Miller and Dr. Qing Ming Wang for taking out the time to be on my Masters committee at such a short notice and providing me with valuable feedback.

Finally, I want to dedicate this work to my parents, my brother and friends for believing in me and my dreams and their encouragement, blessings and support.

1.0 INTRODUCTION

1.1 MOTIVATION

Attachment of dissimilar materials is a major challenge in engineering. Joining two metals is a challenging task and attaching a metal to a plastic or attaching a bone to a ligament is a more challenging problem. The two materials have varied material properties like the elastic modulus and Poisson's ratio and this difference in material properties will have major effect on stresses near the attachments. This will result in regions with higher stresses (Stavros et al., 2006).

The focus in our present study is at the attachment of ligaments to bone. The modulus of elasticity and Poisson's ratio of bone is different from that of the soft tissue ligament, which could result in high stresses at the attachments. The human anterior cruciate ligament (ACL) is the most injured ligament of the body (Fetto and Marshall 1980), especially during sport activities (Speer et al., 1995) and accidents (Crowninshield and Pope 1976). So understanding the stress in ligaments is important to injury of the tissue.

1.2 OBJECTIVE

The objective of present computational study is to study the effect of shape of ligaments on the stresses at bone ligament insertion site.

2.0 STRUCTURE AND FUNCTION OF LIGAMENTS

Ligaments are soft connective tissues that are mainly composed of water, collagen and various amino acids. They are formed by long fibers of collagen. Collagen is composed of groups of proteins and the elasticity of collagen allows ligaments to stretch and then revert to their undeformed shapes when the stress is relieved (K Robi et al., 2013). Ligaments are hypo cellular with interconnected, elongated fibroblastic cells in their mid-substance. The main function of these cells is to maintain the collagen scaffold. Water makes about two-third of the weight of normal ligaments and out of which 70% of the remaining weight is made up of protein (V.C.Mow et al., 2005).

The most important function of the ligaments is to control joint motion. They connect bones and help control movement of the joint by stabilizing it and keeping it from being dislocated. They can be subjected to high forces while performing their role in restricting abnormal joint motion resulting in damage of the ligament due to overloading. However, still the mechanical properties of individual ligaments, the mechanics of ligament injury, and the efficiency of reconstructive procedures are not well known.

2.1 LIGAMENT INSERTION

Ligament insertion sites transmit loads to a bone and are hypothesized to be formed in such a way to reduce the stresses that occur at ligament and bone interfaces (Benjamin et al, 2006). The insertions of a ligament to bone are biomechanically complex. The structure and shape of the insertion site is different for each ligament and also at the two ends of same ligament. There are said to be two types of insertions direct and indirect.

At indirect insertion sites, the fibers attach to bone with little or no transitional zone. The collagen fibers meet bone at acute angles and there is an interface line separating the mineralized and non-mineralized tissues. This ligament insertion type is characterized by the progression of collagen fibers that attach into periosteum and sub chondral bone without gradual transition (Freddie H. Fu et al., 2008).

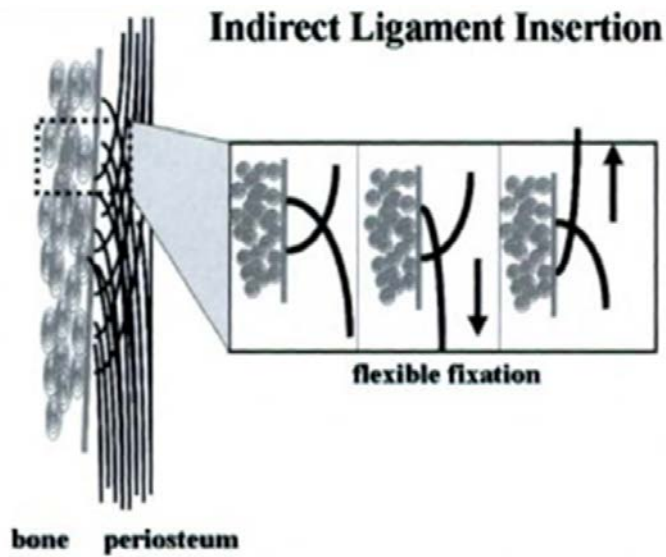


Figure 1: Indirect Ligament Insertion (Freddie H. Fu et al., 2008)

Direct insertion sites are areas of attachment where bone and attaching ligament occur over a distance of less than 1mm and consist of a distinct right-angle boundary where collagen fibers extend out (Suvaranu De et al., 2014). The collagen fibrils quickly pass out of normal ground substance matrix and continue through zones of fibrocartilage, mineralized fibrocartilage and finally into bone (Cooper et al., 1970). The direct insertion of the ACL carries more load than the indirect insertion (D.H. Nawabi et al., 2014).

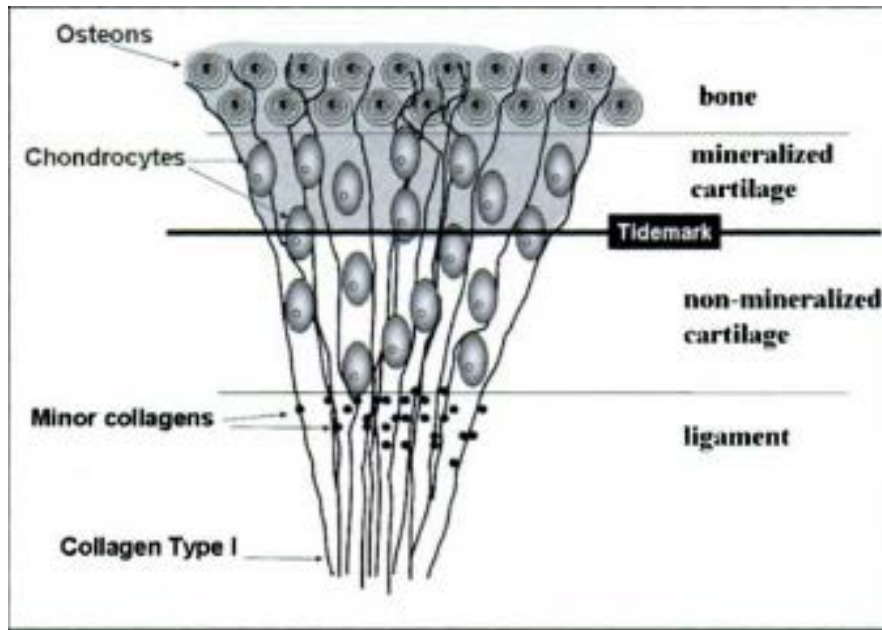


Figure 2: Direct Ligament Insertion (Freddie H. Fu et al., 2008)

In Figure 3, the shape of the ligament where it attaches to bone is shown (Kevin D. Plancher et al., 2005).

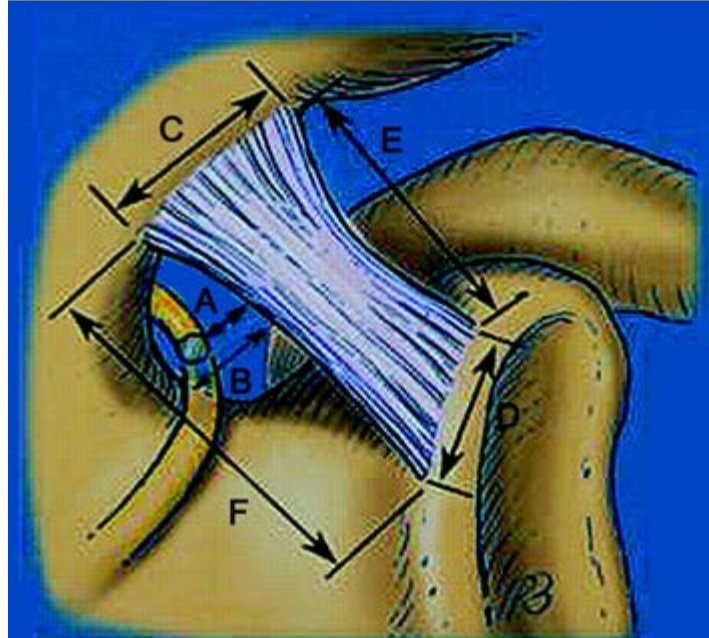


Figure 3: Shape of ligament where it attached the bone (Kevin D Plancher et.,al 2005)

From Figure 3, we note that the ligament can have different shapes and sizes depending on various parameters.

3.0 BACKGROUND

The most common method of modeling ligaments was using one-dimensional discrete line elements, which act as tension only springs (Panzer and Cronin 2009). This method was used to model the system level models as it reduces the complex mechanics of the ligaments to that of a spring but still allowing for the prediction of joint kinematics. The main disadvantages of this method were it could not predict the stress in the ligament tissue and the load cannot be transferred between the ligament and surrounding tissues. Later two dimensional computational models of ligaments were used which predicted the shear and compressive loading which was not predicted by the one- dimensional representation. A two-dimensional, plane stress finite element model of the rabbit ligament in the mid-coronal plane was developed by Matyas et al. 1995 using experimentally determined geometry. The three dimensional ligament models (Weiss 2005; Pioletti's 1998) are used for the detailed analysis of the ligament to predict the mechanics of ligament and understand the stresses in various tunnel positions. Curves describing the external geometry of the insertion sites were determined experimentally and a solid was created to join the two curves. Two approaches namely, a realistic approach and an artificial approach were followed while modeling three dimensional ligament models. In the artificial method, the geometry of the ligament was assumed to have a constant cross section throughout the length, whereas, in realistic approach the geometry of the ligament by digitizing the fiber

bundles of the ligament and using cubic spline interpolation to fill the remaining geometry (Zhang 2008).

There were no previous researches or studies on the shape of the ligament geometry and how it will effect the stresses at the insertion sites. Also the shape of the ligament geometry was not focused in any previous research.

4.0 MATERIAL PROPERTIES OF LIGAMENTS

Ligaments are anisotropic, non-linear materials normally subjected to complex loadings (Giori et al., 1993). The fiber orientations in the ligament is thought to represent an adaptation to the mechanical loading of ligament and are generally aligned with the long major axis (Zhang 2008). Primary resistance to tensile loading is provided by the collagen fibers, which do not provide any resistance to compression (Zhang 2008). Experimental data has shown the load-elongation curve for ligaments to have a nonlinear section at low levels of strain and then a linear region until it reaches yield point. It is thought that the initial nonlinear section is due to the fact that in a zero strain position, the collagen fibers are in a crimped configuration, and at a low load the fibers are in the act of straightening, resulting in a nonlinear load-elongation curve until the fibers are completely straightened, at which point the load-elongation curve becomes linear (J.A. Weiss 2001). The ligament apart from exhibiting nonlinear elastic responses also exhibit visco-elastic properties which are dependent on time and history. This arises due to interaction of ground substance matrix with water. A typical force- deformation curve for the ligaments where load is applied in a uni-axial direction along the fibers direction is shown in Figure 4 (Martin 1998).

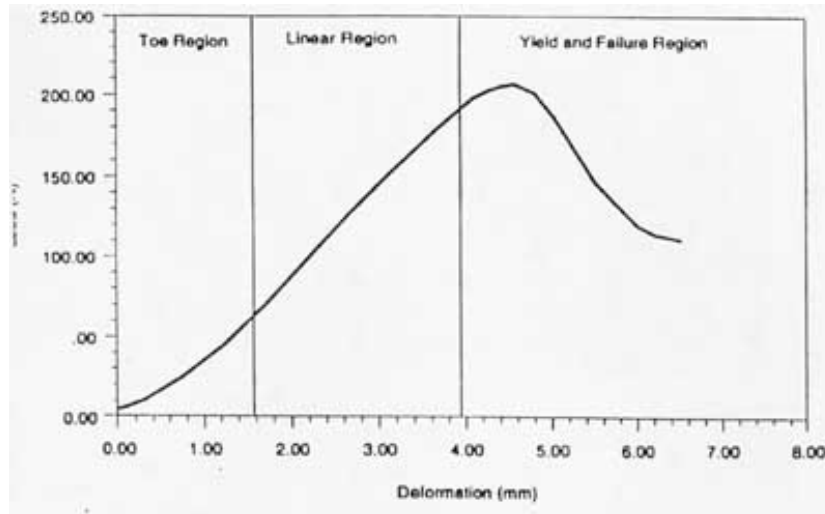


Figure 4: Force - Deformation curve for ligaments (Martin 1998)

4.1 MATERIAL MODELS

To represent the mechanical behavior of ligaments, continuum models have been developed. These constitutive equations are used to describe stress-strain behavior of materials through specification of the dependence of stress on variables, such as deformation gradient, rate of deformation. It is still a challenge to accurately predict the mechanical behavior of ligaments. An approach to describe the material behavior of ligament is to fit the mathematical equations in experimental data. One method is to characterize the ligament as hyper-elastic material. A hyper-elastic material is a subclass of an elastic material and is a constitutive model for in which the stress-strain relationship derives from a strain energy density function.

The most influential model that was developed for modelling the biological tissues is Holzapfel-Gasser-Ogden (HGO) model (Holzapfel 2000). In this model the strain energy (W) is given by:

$$W = \frac{c}{2}(I_1 - 3) + \frac{k_1}{k_2}(e^{k_2(I_4 - 1)^2} - 1) \quad (3.1)$$

where, I_1 and I_4 are strain invariants defined as $I_1 = \text{trace}(C)$ and $I_4 = M \cdot (CM)$, C is the Cauchy-Green tensor and c , k_1 and k_2 are the material parameters of ligament. M is the unit vector pointing in the direction of tissue fibers before any deformation.

Limbert represented the ligament as a transversely isotropic hyper-elastic material [18] (Limbert 2001) whose strain energy function took the following form, which was originally developed by Weiss (1996) as:

$$W = F_1(\tilde{I}_1) + F_2(\tilde{\lambda}) + \frac{K}{2} * \ln(J)^2 \quad (3.2)$$

where the strain energy function was split up in contributions from the ground substance (F_1) and the fibers (F_2), (\tilde{I}_1) is the first deviatoric invariant of the deformation tensor, $(\tilde{\lambda})$ represents the deviatoric part of stretch along collagen fiber direction, (K) is the bulk modulus and (J) is the determinant of the deformation tensor. In this model, the ground substance was modeled as incompressible and isotropic and was regarded as a Neo-Hookean model whose strain energy function was described as:

$$F_1 = \frac{1}{2} * C_1 * (\tilde{I}_1 - 3) \quad (3.3)$$

where C_1 is constant of Neo Hookean model. As the collagen fibers do not support compressive load, the tensile stretch relationship is characterized by a piece wise continuous function. The strain energy function for the collagen fibers (F_2) is formulated as:

$$\begin{aligned}
& F_2(\tilde{\lambda}) \\
& = \int \frac{\partial F_2}{\partial(\tilde{\lambda})} d\tilde{\lambda} \text{ such that } \begin{cases} \frac{\partial F_2}{\partial \tilde{\lambda}} = 0 & \text{if } \tilde{\lambda} \leq 1 \\ \frac{\partial F_2}{\partial \tilde{\lambda}} = \frac{C_2}{\tilde{\lambda}} [e^{C_3(\tilde{\lambda}-1)} - 1] & \text{if } \tilde{\lambda} \geq 1 \end{cases} \quad (3.4)
\end{aligned}$$

where C_2 is a factor that scales the exponential stress and C_3 controls the rate of un-crimping of collagen fibers.

The Ogden model expresses the strain energy function W in terms of principal stretches λ_1 , λ_2 and λ_3 . Formulation for the model has μ_p and α_p as material constants (Ogden 1972) and is given by:

$$W = \sum_{p=1}^n \frac{\mu_p}{\alpha_p} * (\lambda_1^{\alpha_p} + \lambda_2^{\alpha_p} + \lambda_3^{\alpha_p} - 3) \quad (3.5)$$

Later Pioletti (1998) developed an isotropic hyper elastic constitutive law for ligaments in conjunction with an elastic potential developed by Veronda and Westmann (1970) originally proposed to model finite deformations of the skin in which α , β and C_1 are material constants of ligament as

$$W = \alpha * e^{[\beta(I_1-3)]} + C_1(I_2 - 3) \quad (3.6)$$

Another model which is commonly used to model hyper elastic material is polynomial model introduced by Rivlin & Sanders (Rivlin et al., 1951). It is formulated in terms of the first and second strain invariants of the Cauchy-Green deformation tensor, with C_{ij} denoting material constants. This model is called as Generalized Rivlin Model (Chang et al., 1991) and is given by

$$W = \sum_{i=0}^n \sum_{j=0}^n C_{ij} * (I_1 - 3)^i * (I_2 - 3)^j \quad (3.7)$$

In our current study the Pioletti's constitutive model for a ligament (Equation 3.6) which is widely adopted by other investigators (Debski et al., 2004; Pena et al., 2006) is used for the modelling the ligament as this was based on an incompressible isotropic hyper-elastic formulation for ACL and the elastic parameters were determined from curved fitting the experimental data obtained from the uniaxial tensile tests on human anterior cruciate ligament (ACL). The results of this model showed good correlation between experimental and theoretical curves over a range of strain rates (Pioletti 1998).

5.0 FINITE ELEMENT ANALYSIS

The equations of motion can be combined with a suitable constitutive model to obtain mathematical solutions to problems with relatively simple geometry and boundary conditions. But most of the time with a complex geometry and arbitrary boundary and loading conditions solving these mathematical equations is not easy, so finite element computational analysis is used. This method offers ability to predict spatial and temporal variations in stress, strain and contact area/forces (Weiss 2005).

5.1 CONSTITUTIVE MODEL OF LIGAMENTS

The strain energy function proposed by Pioletti (1998) is difficult to implement in Ansys finite element analysis software as the software cannot accept the material constants of the ligament in this form (ANSYS Inc. User Manual). So the above strain energy equation (Equation 3.6) was modified into a polynomial form. The values of material constants α , β and C_1 in the Pioletti equation (Equation 3.6) are obtained from the literature which were experimentally calculated from the stress strain curve of a human ligament. The values for material constants for the anterior cruciate ligament (ACL) are $\alpha = 0.26$, $\beta = 11.35$ and $C_1 = -1.49$. (Pioletti 1998).

$$W = \alpha * e^{[\beta(I_1-3)]} + C_1(I_2 - 3) \quad (4.1)$$

Taking $x = I_1-3$, expanding the terms of Pioletti equation using Taylor series expansion (Abramowitz 1970)

$$\alpha * e^{(\beta x)} = \alpha \left(1 + \beta x + \frac{(\beta x)^2}{2!} + \frac{(\beta x)^3}{3!} + \frac{(\beta x)^4}{4!} + \dots \right) \quad (4.2)$$

Expanding and calculating the coefficients results in $\alpha = 0.26$; $\alpha * \beta = 2.95$; $\alpha * \beta^2 / 2! = 16.74$ and $\alpha * \beta^3 / 3! = 63.35$, substituting the values into equation 4.2 gives

$$W = 0.26 + 2.95*x + 16.74*x^2 + 63.35*x^3 - 1.49*(I_2 - 3) \quad (4.3)$$

When the above equation is compared to the cubic polynomial model form (Equation 3.7),

$$W = C_{10}*(I_1-3) + C_{20}*(I_1-3)^2 + C_{30}*(I_1-3)^3 + C_{01}*(I_2-3) \quad (4.4)$$

we get the coefficients of the first, second and third order terms of the polynomial as 2.95, 16.74 and 63.35 respectively which translates to the values of the coefficients of $C_{10} = 2.95$; $C_{20} = 16.74$; $C_{30} = 63.3592$ and $C_{01} = -1.49$ respectively.

To check the difference between the cubic polynomial approximation and the exponential equation, the graphs of strain energy functions were plotted for strain energy vs strain (figure 4) for the Pioletti equation and the polynomial model. W_1 is the strain energy function form proposed by Pioletti and W_2 is strain energy function in cubic polynomial form.

$$W_1 = (0.26 * e^{(11.35x)}) \quad (4.5)$$

$$W_2 = 2.95 * x + 16.7463 * x^2 + 63.3592 * x^3 + 0.26 \quad (4.$$

From the graph in Figure 5, difference between the energy values of cubic polynomial and Pioletti models below the strain value of 0.156 is less than 9.6%. So the new model can be used to model the ligament in finite element analysis.

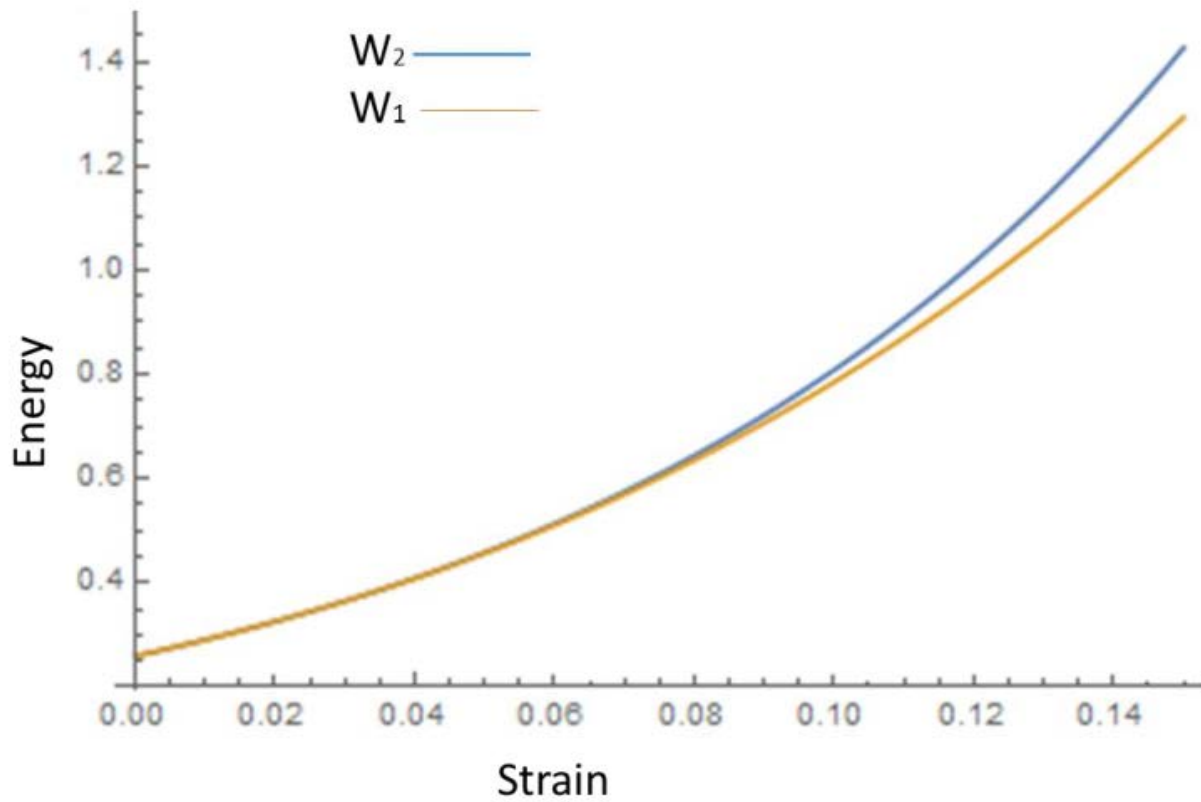


Figure 5: Strain energy vs strain for cubic polynomial model (W_2) and Pioletti model (W_1)

6.0 APPROACH & ANALYSIS

A non-linear finite element analysis (FEA) was performed to model the ligament. A commercial finite element software (ANSYS v15) was used to evaluate the stresses and displacements due to the applied load. The bone was assumed to be a rigid material and the ligament was attached to it. Only the ligament was modeled for finite element analysis. A parametric study was done on the effect of various ligament geometries was studied. A two dimensional axisymmetric model is used to model the ligament.

6.1 BOUNDARY AND LOADING CONDITIONS

One end of the ligament was taken to be rigidly fixed with all degrees of freedom constrained and uniform tensile stress was applied at the other end. A uniform load of 200N (F) is applied on the right edge (R) of the 2D model and left edge of the ligament (C) is constrained in all degree of freedom. The top edge of the model is along the axis of symmetry as shown in Figure 6. The Poisson's ratio of the ligament was considered as 0.45 (Ozkaya & Nordin 1999).

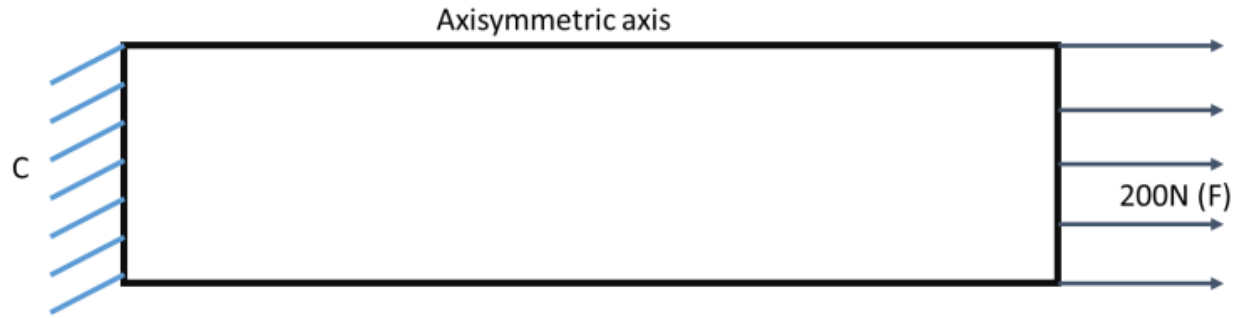


Figure 6: Boundary and load conditions on the ligament

6.2 GEOMETRY OF LIGAMENT

The length of ligament was taken to be 30 mm. Different cylindrical shapes of ligaments were modelled by changing the shape parameters. The shapes of the cylinder can be modified by changing fillet radius or fillet angle or using different edge lengths at both the ends or changing the curve of the cylindrical height can be modified to create new geometries. Many different shapes can be created from a cylinder but in our present study we are considering four shapes which may affect the stresses at the insertion sites. The five different shape cases which were modeled and analyzed using FEA are:

Case I: Variable Edge length (Straight Cylinder)

The length of ligament is fixed as 30mm. The diameter of the cylinder is varied from 10mm to 20mm in intervals of 2mm.

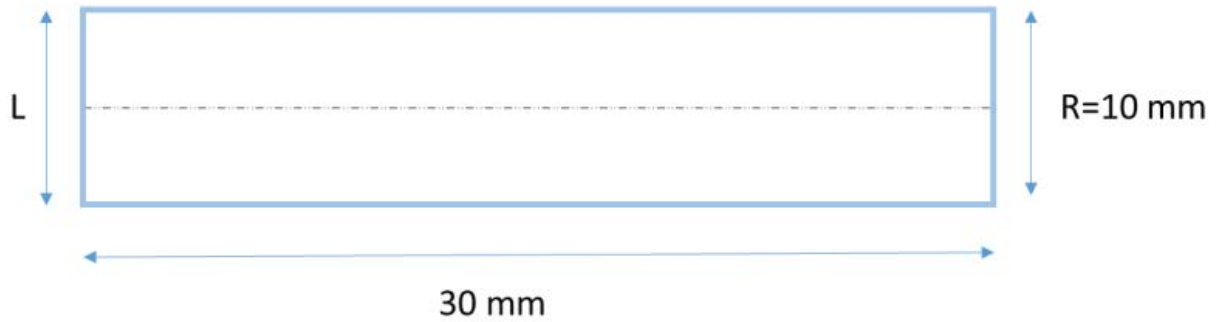


Figure 7: Ligament geometry for Case I

Case II: Variable Edge length (Tapered Cylinder)

The length of ligament is fixed as 30mm and the right edge length (R) is fixed to be 10mm. The left edge (L) of the cylinder is varied from 10mm to 20mm as shown in Figure 8.

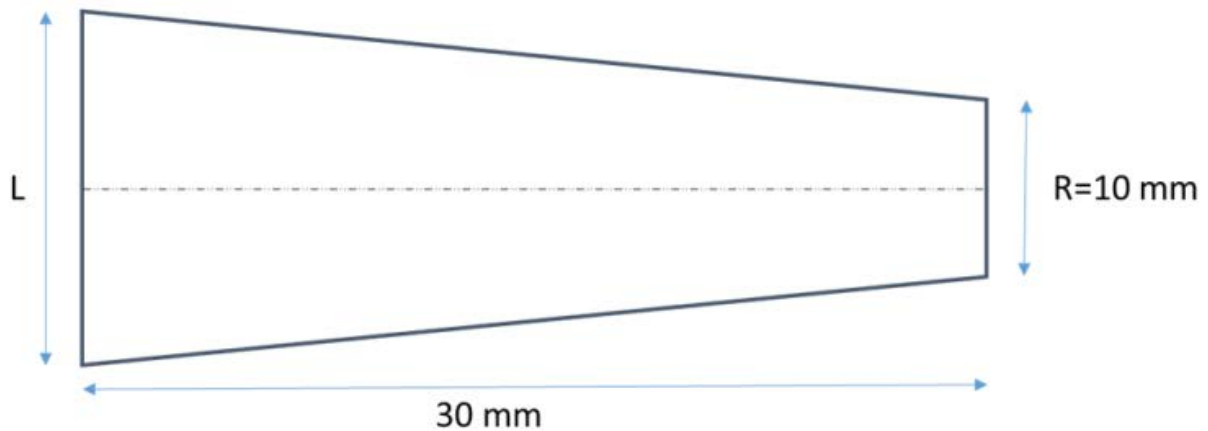


Figure 8: Ligament geometry for Case II

Case III: Variable Fillet Radius

The length of ligament is fixed at 30mm and the right edge length (R) is fixed to be 10mm. The fillet radius (F) of the cylinder is varied from 5mm to 1mm and the left edge length (L) is adjusted accordingly as shown in Figure 9.

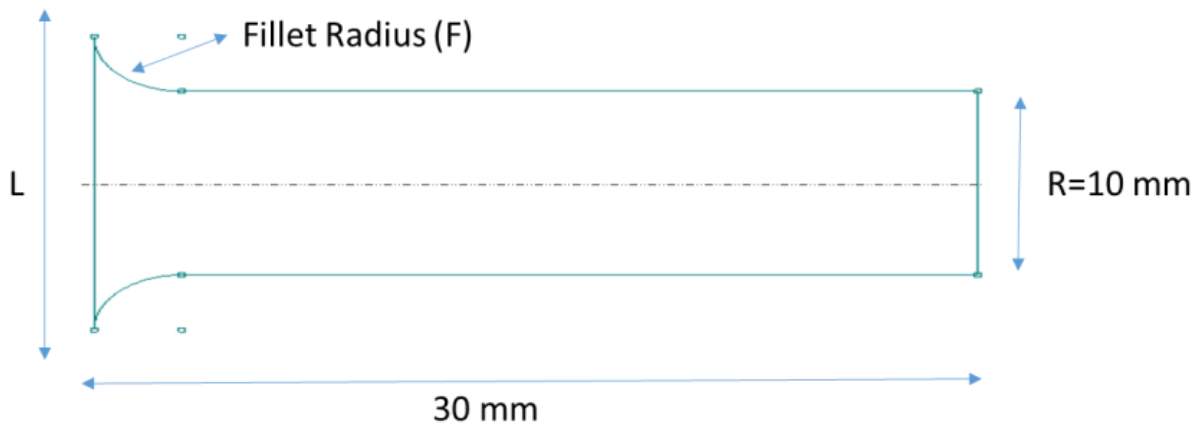


Figure 9: Ligament geometry for Case III

Case IV: Variable Angle (fillet angle)

The length of ligament is 30mm and the right edge length (R) is 10mm. The left edge length (L) of the cylinder is fixed as 20mm and the fillet angle (A) of the cylinder is varied from 30 degrees to 75 degrees and the length of the straight section is adjusted accordingly as shown in the Figure 10.

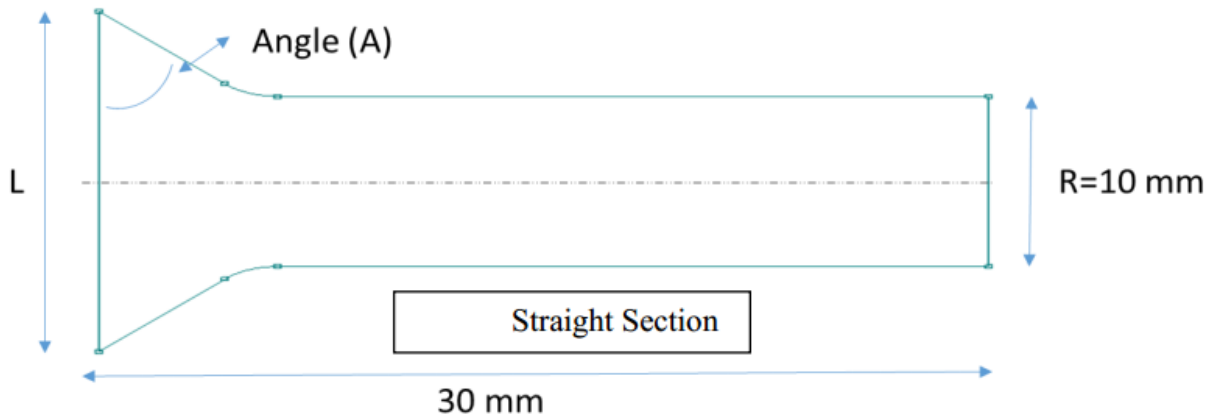


Figure 10: Ligament geometry for Case IV

Case V: Variable Minor Radius

The length of ligament is 30mm and the right edge length (R) is set at 10mm. The minor radius elliptical right hand side from 6mm to 10 mm and the left edge length (L) is adjusted accordingly based on the major axis that was decided based on the variable radius as shown in Figure 11.

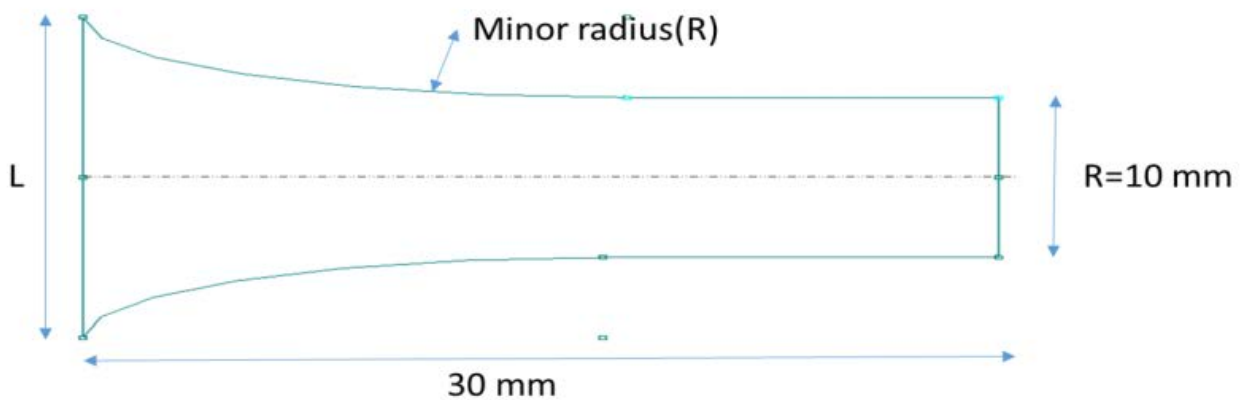


Figure 11: Ligament geometry for Case V

6.3 FINITE ELEMENT MESHING

Two-dimensional axisymmetric quadrilateral elements are used in the model. The model was meshed with an element size of 0.09 after evaluating the mesh sensitivity of the ligament model. Sample meshed model of ligament for each of the five cases is shown below in Figures 12-16.

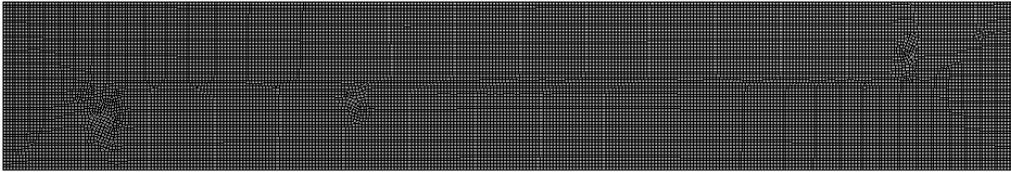


Figure 12: Meshed model of the ligament for Case I

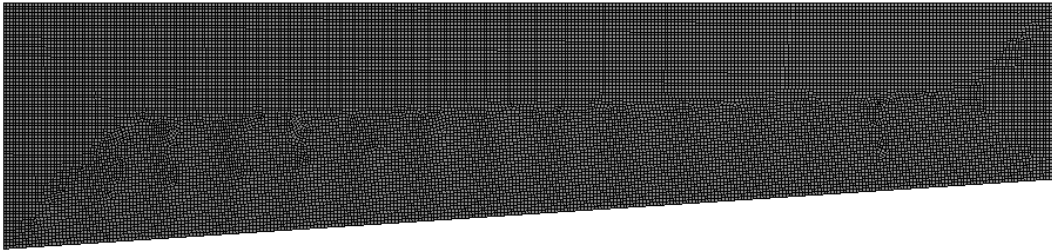


Figure 13: Meshed model of the ligament for Case II

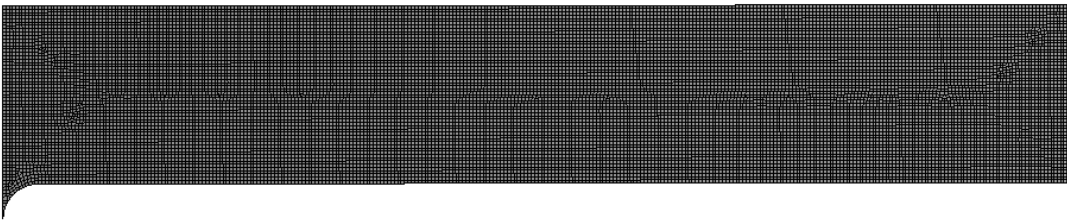


Figure 14: Meshed model of the ligament for Case III

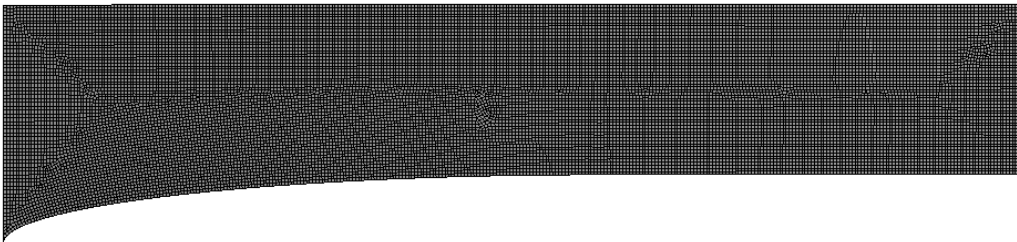


Figure 15: Meshed model of the ligament for Case IV

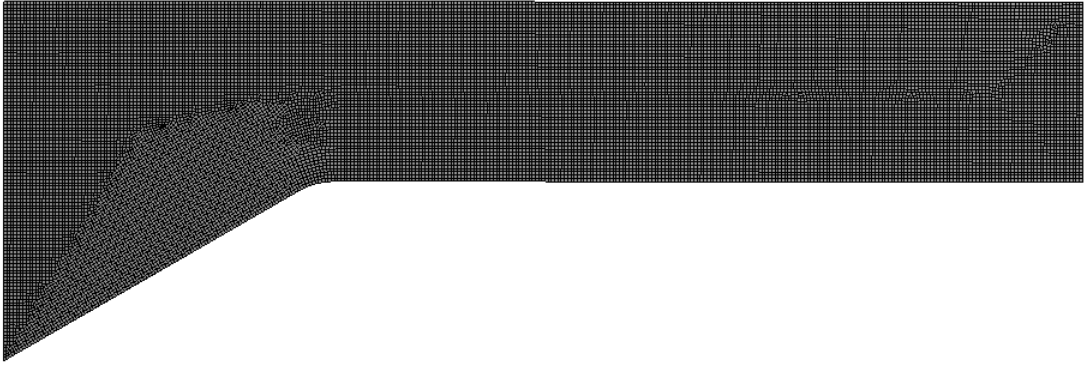


Figure 16: Meshed model of the ligament for Case V

7.0 RESULTS AND DISCUSSION

The goal of the computational analysis was to provide insight into the effect of the shape parameters of ligament have on the stresses and displacement. In the following section, the stress results will be discussed for comparison across different shape parameters and the effect of element size. Three different mesh sizes were studied to see the effect of mesh on the stress and displacement. The analysis was performed for element sizes of 0.07, 0.09 and 0.25 mm.

7.1 EFFECT OF VARYING DIAMETER

With this geometry, the diameter of the cylinder was varied from 10mm to 20 mm in the increments of 2 mm and 6 different cases were studied. A sample case is shown below in Figures 17.



Figure 17: Case I with diameter of 10 mm

Figures 18-19 compare the end displacement and maximum von mises stress results of the finite element analysis for different diameter (D) for element size of 0.09. As diameter increases the displacement and von Mises stress decreases. Values of the maximum von Mises stress, maximum normal stress in axial and radial direction and end displacement along with the location where the maximum stress are shown along with the number of nodes and elements in Appendix B. The maximum stress values are found when the ligament diameter is 10mm.

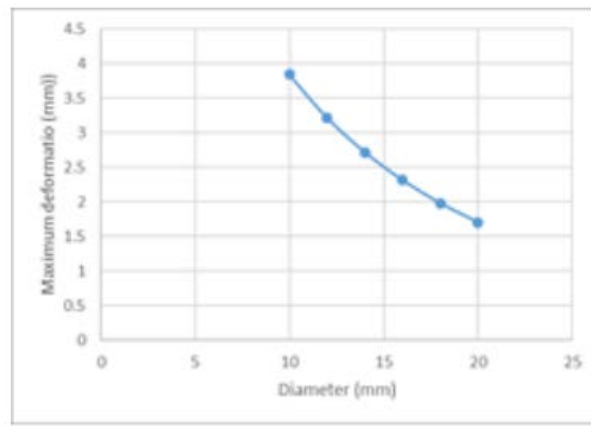


Figure 18: Maximum displacement vs diameter

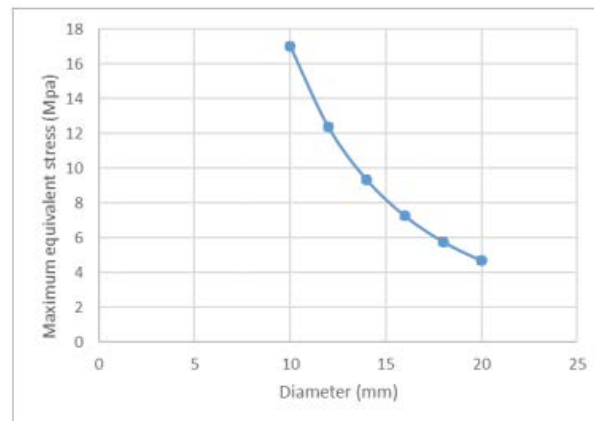


Figure 19: Maximum von Mises stress vs diameter

Figures 20-22 shows the effect of the diameter on the normal radial, axial stress and shear stress. The normal stress in the radial and axial direction decreases with increase in diameter. The shear stress also decreases as we increase the diameter.

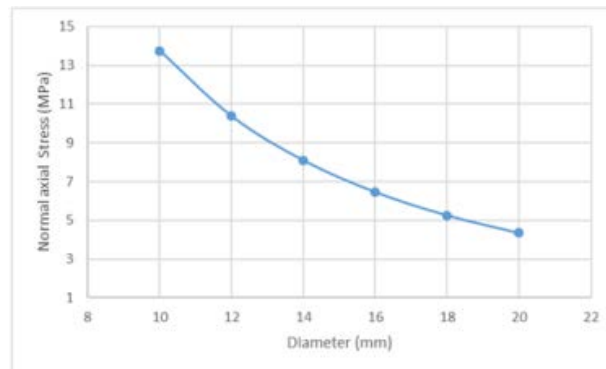


Figure 20: Normal axial stress vs diameter

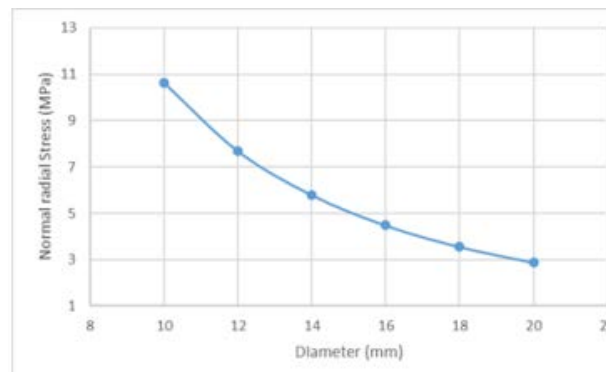


Figure 21: Normal radial stress vs diameter

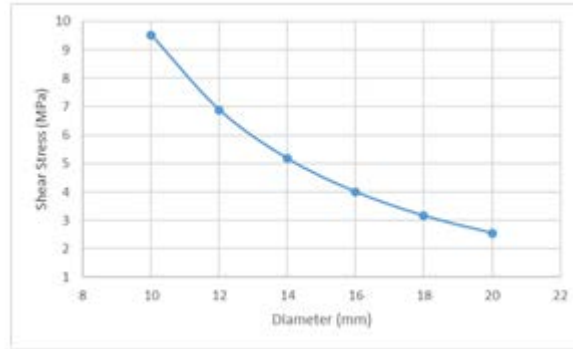


Figure 22: Maximum shear stress vs diameter

Plots of the distributions of the von Mises stress, normal axial stress, shear stress and normal radial stress for the diameter of 14mm are shown in Figures 23-26.



Figure 23: von Mises stress (MPa) plot for Case I (Diameter 10mm)



Figure 24: Normal axial stress (MPa) plot for Case I (Diameter 10mm)



Figure 25: Normal radial stress (MPa) plot for Case I (Diameter 10mm)

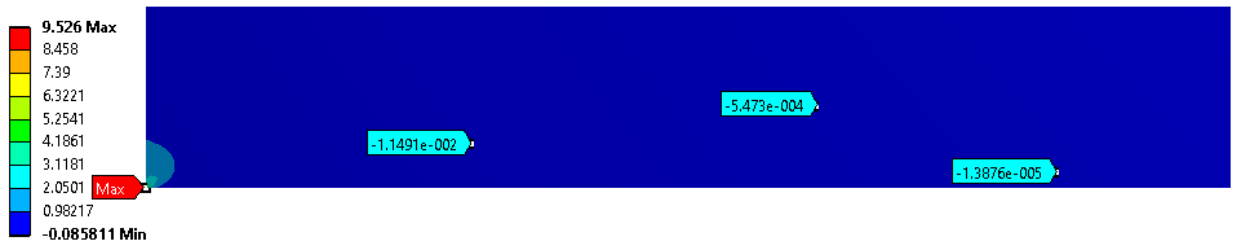


Figure 26: Shear stress (MPa) plot for Case I (Diameter 10mm)

In the Table 1, the maximum stress values along with the location of the maximum stress are shown for element size of 0.09. The maximum stresses are located at the corner as shown in the Figures 23-26.

Table 1: Maximum stress values and location for case I (Element size 0.09)

Diameter (mm)	No of nodes	No of elements	Maximum displacement (mm)	Max equivalent stress (MPa) / Location	Max Shear stress(MPa) /Location	Max Normal axial stress (MPa)/ Location	Max Normal radial stress(MPa) / Location
10	53892	17721	3.841	17.011	9.526	13.753	10.617
12	64093	21114	3.216	12.361	6.889	10.381	7.6774
14	74823	24684	2.718	9.335	5.178	8.098	5.7880
16	86183	28458	2.313	7.254	4.004	6.463	4.4806
18	98450	32537	1.979	5.765	3.167	5.261	3.5594
20	111173	36766	1.702	4.669	2.554	4.352	2.8820

Mesh sensitivity studies were performed and Figures 41-44 show the effect of the different element sizes on the ligament stresses and displacement when the diameter is varied.

There is no variation in the displacement when the mesh size is changed. Figures 41-44 shows that von Mises stress and normal stress values increases as we decrease the element size from 0.09 to 0.07 and decreases if we increase the element size from 0.09 to 0.25 which shows that the stress is mesh dependent. The stress increases with the increase the mesh size and also the there is only a small variation in the stress values for different mesh sizes as the diameter increases so the mesh size is adequate for the analysis.

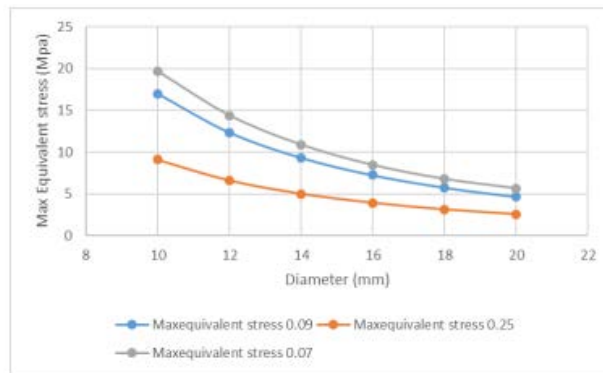


Figure 27: Mesh sensitivity for von Mises stress

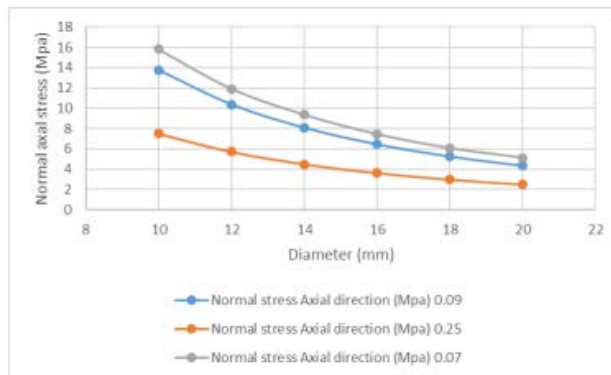


Figure 28: Mesh sensitivity for normal axial stress

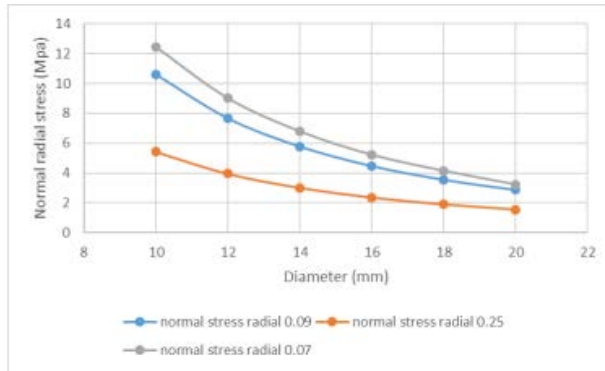


Figure 29: Mesh sensitivity for normal radial stress

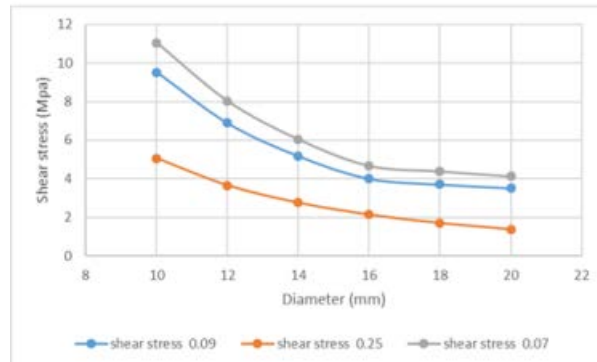


Figure 30: Mesh sensitivity for shear stress

7.2 EFFECT OF VARIABLE EDGE LENGTH

With this geometry, the left edge length was varied from 10mm to 20 mm in the increments of 2 mm and 6 different cases were studied. Two sample cases are shown below in Figures 31-32.



Figure 31: Case II for edge length 6mm



Figure 32: Case II for edge length 10mm

Figures 33-34 compare the end displacement and maximum von mises stress results of the finite element analysis for different edge length (L) for element size of 0.09. As edge length increases the displacement and stress decreases. Values of the maximum von Mises stress, maximum normal stress in axial and radial direction and end displacement along with the location where the maximum stress are shown along with the number of nodes and elements in Appendix B.

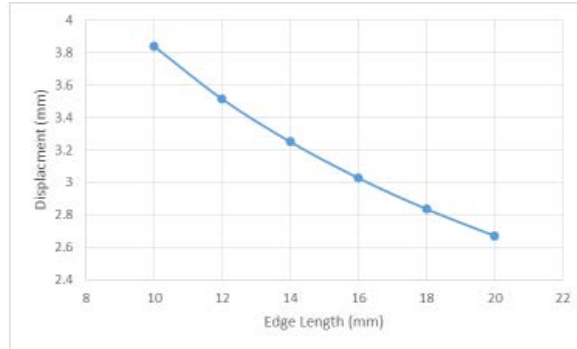


Figure 33: Maximum displacement vs edge length

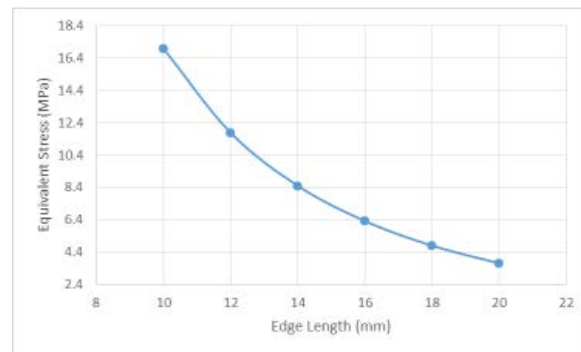


Figure 34: von Mises stress vs edge length

Figures 35-36 shows the effect of the edge length on the radial and axial stress. The normal stress in the radial and axial direction decreases with increase in edge length. The shear stress also decreases as we increase the edge length and it is maximum at the corner location and in the surrounding area it is nearly equal to 0 MPa.

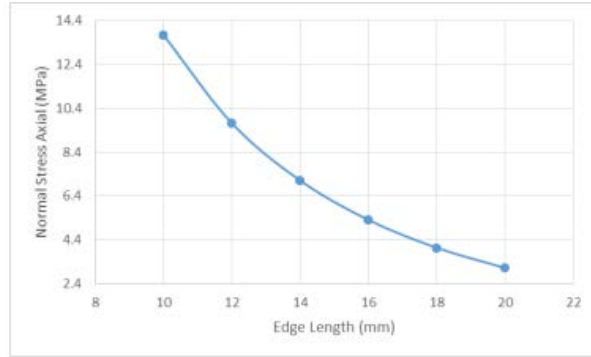


Figure 35: normal axial stress vs edge length

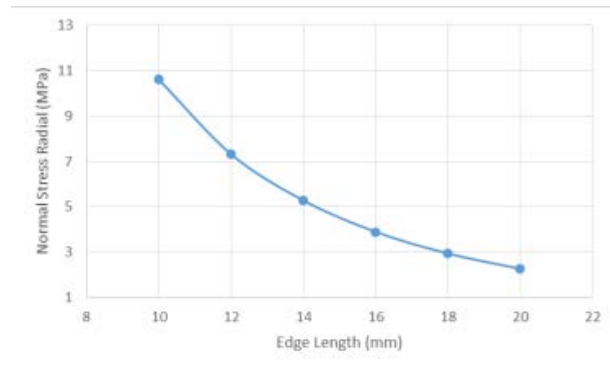


Figure 36: normal radial stress vs edge length

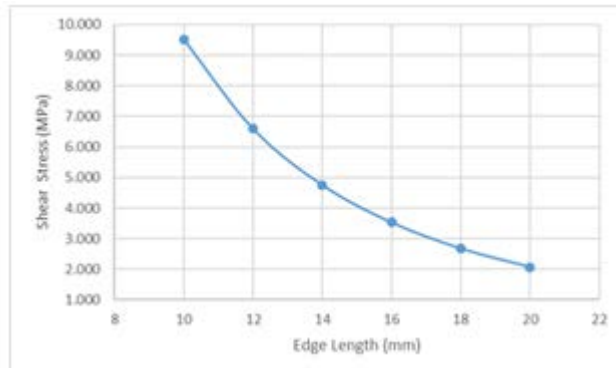


Figure 37: maximum shear stress vs edge length

Plots of the distributions of the von Mises stress, normal axial stress, shear stress and normal radial stress for the edge length of 7mm are shown in Figures 38-41.

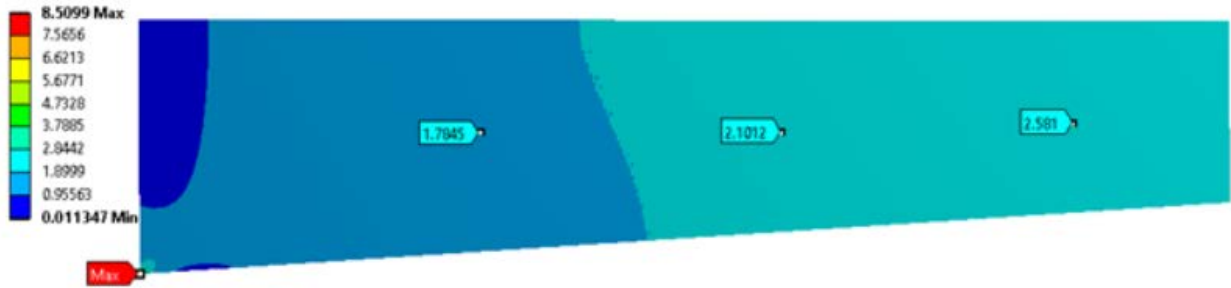


Figure 38: von Mises stress (MPa) plot (Edge length 7mm)

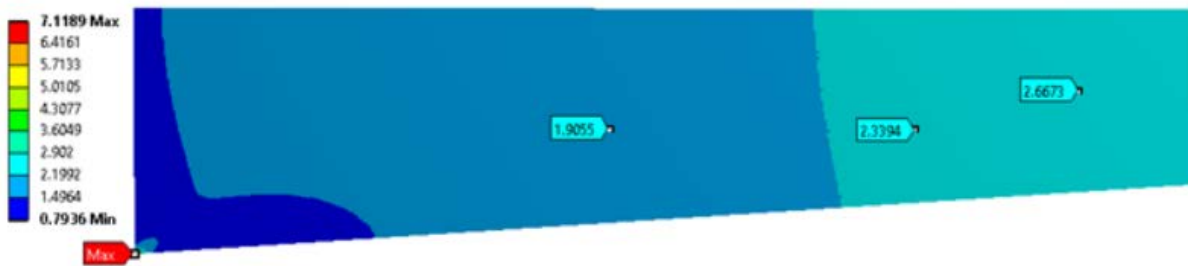


Figure 39: Normal axial stress (MPa) plot (Edge length 7mm)

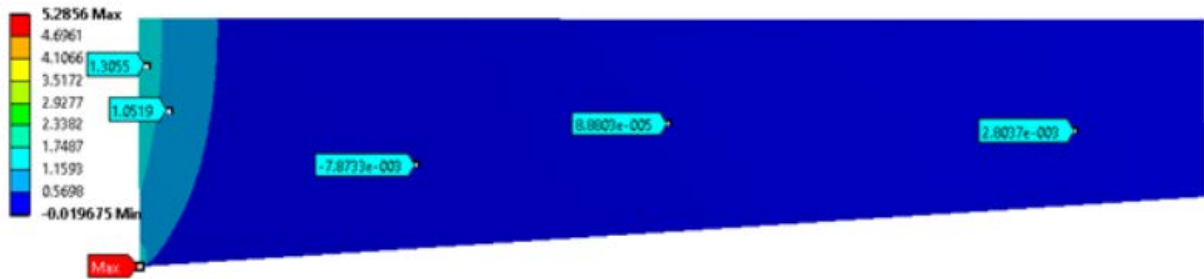


Figure 40: Normal radial stress (MPa) plot (Edge length 7mm)

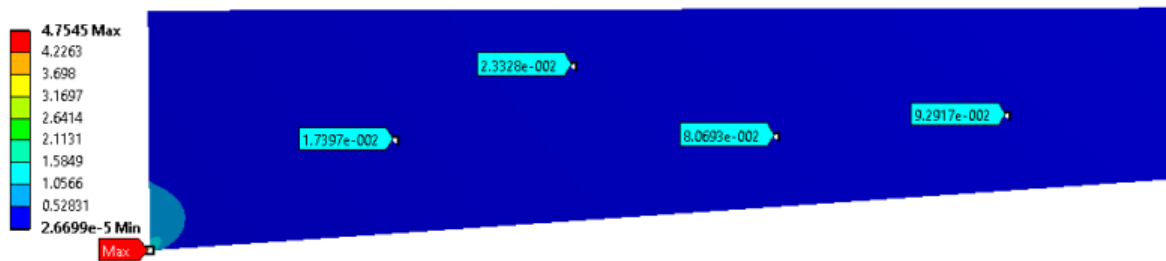


Figure 41: Shear stress (MPa) plot (Edge length 7mm)

In the Table 2, the maximum stress values along with the location of the maximum stress are shown for element size of 0.09. The results for element size 0.07 and 0.25 are shown in Appendix B-a. The maximum stresses are located at the corner as shown in the Figures 38-41.

Table 2: Maximum stress value and locations for case II

<u>Edge length (mm)</u>	<u>No of nodes</u>	<u>No of elements</u>	<u>Maximum displacement (mm)</u>	<u>Max von Mises stress (MPa) / Location</u>	<u>Shear stress (MPa) / Location</u>	<u>Normal stress (MPa) / Axial direction / Location</u>	<u>Normal stress (MPa) / Radial direction / Location</u>
10	53892	17721	3.8413	17.011/ Corner	9.526 / Corner	13.754 / Corner	10.617/ Corner
12	59176	19477	3.5147	11.798/ Corner	6.596/ Corner	9.733/ Corner	7.326/ Corner
14	65274	21505	3.251	8.509/ Corner	4.754/ Corner	7.118/ Corner	5.285/ Corner
16	71674	23637	3.0273	6.321/ Corner	3.530/ Corner	5.316/ Corner	3.900/ Corner
18	78907	26044	2.8356	4.797/ Corner	2.679/ Corner	4.044/ Corner	2.946/ Corner
20	85819	28346	2.6704	3.707/ Corner	2.071/ Corner	3.123/ Corner	2.268/ Corner

Mesh sensitivity studies were performed. Figures 42-45 show the effect of different element sizes on ligament stresses due to varied edge length. There is no or slight variation in the displacement when the mesh size is changed. Figures 42-45 shows that von Mises and normal stress values are increased as the element size decreases from 0.09 to 0.07 and decreases if we increase the element size from 0.09 to 0.25 which shows that the stress is mesh dependent. The stress values decreases with the increase in edge length and also the there is only a small variation in the stress values for different mesh sizes as the edge length increases so the mesh size is adequate for the analysis.

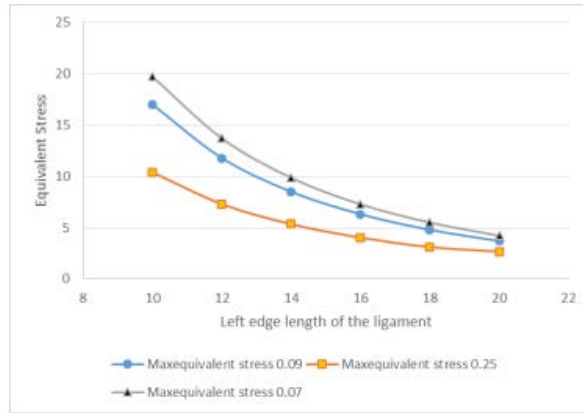


Figure 42: Mesh sensitivity for von Mises stress

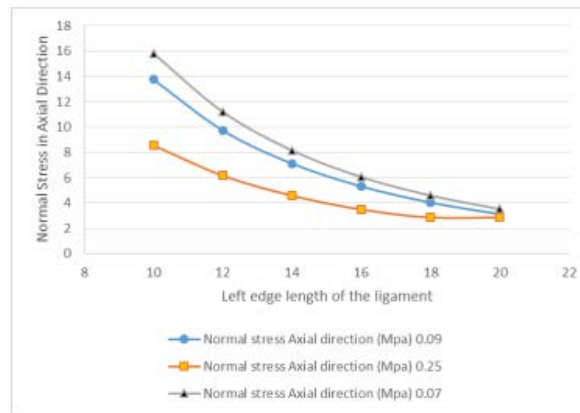


Figure 43: Mesh sensitivity for normal axial stress

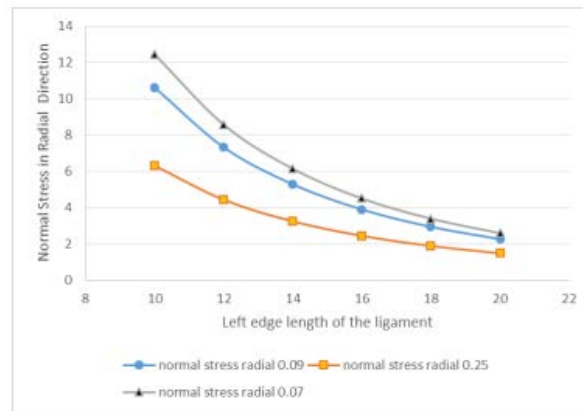


Figure 44: Mesh sensitivity for normal radial stress

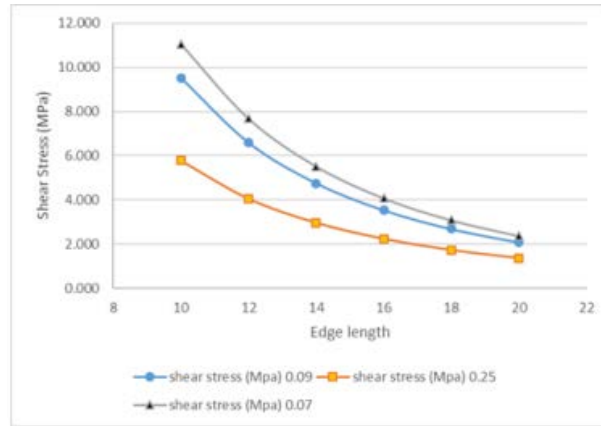


Figure 45: Mesh sensitivity for shear stress

7.3 EFFECT OF VARYING FILLET RADIUS

With this geometry, the fillet radius was varied from 1mm to 5 mm in the increments of 1 mm and five different cases were studied. Two sample cases are shown below in Figures 46 -47.



Figure 46: Case III with fillet radius 1mm



Figure 47: Case III with fillet radius 5mm

Figures 48-52 gives the results of the finite element analysis for different fillet radius for an element size of 0.09. As fillet radius increases the displacement decreases. Values of the maximum equivalent stress, normal stress in axial and radial direction and end displacement along with the location where the maximum stress values are shown in Appendix B-b.

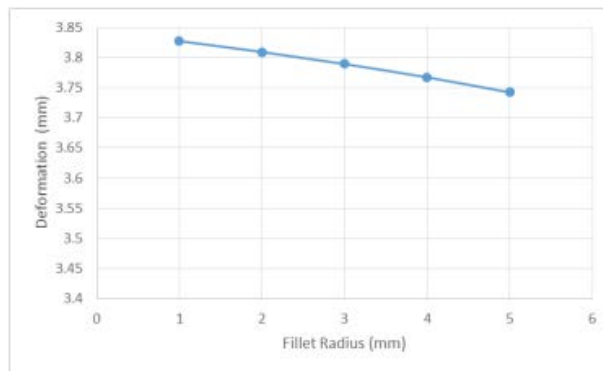


Figure 48: Maximum displacement vs fillet radius

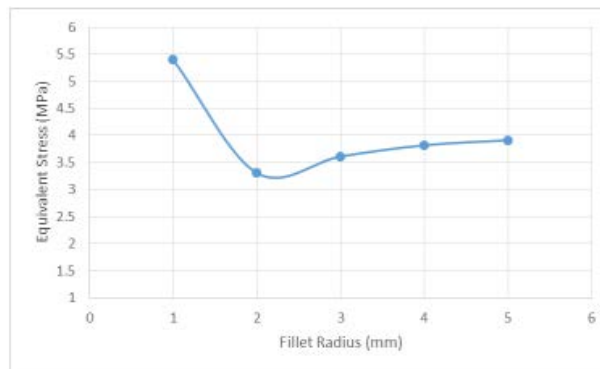


Figure 49: von Mises stress vs fillet radius

Figures 50-51 show the effect of the fillet radius on the normal stress in radial and axial direction. The normal stress decreases when the fillet radius is increased from 1mm to 2 mm but increases from 2mm to 5mm, this is because of development of higher stress concentration in fillet radius of 1mm which has a smaller arc and higher element density in that fillet location and also the maximum stress occurs at the middle of the circle instead of at the transition area.

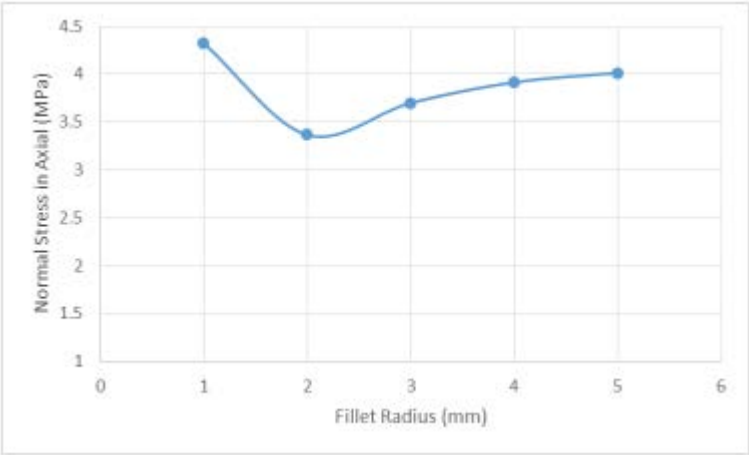


Figure 50: Normal axial stress vs fillet radius

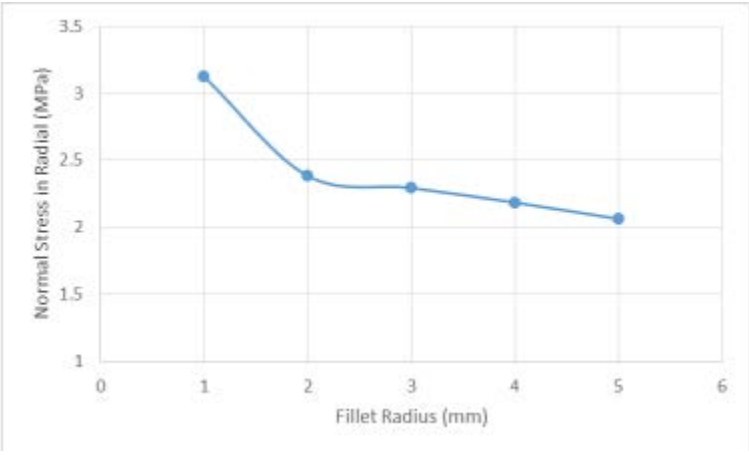


Figure 51: Normal radial stress vs fillet radius

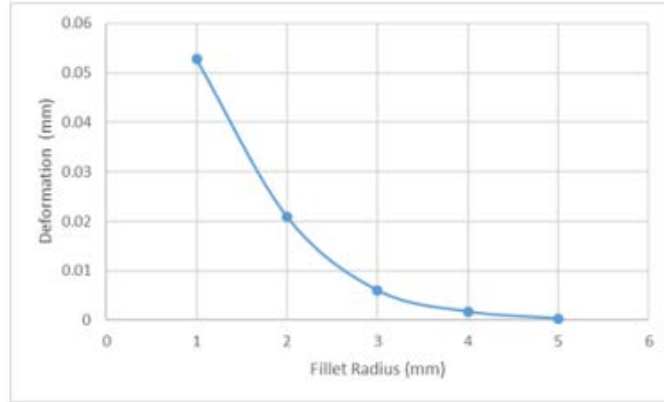


Figure 52: Shear stress vs fillet radius

Plots of the distributions of the von Mises stress, normal axial stress, shear stress and normal radial stress for the fillet radius of 4mm are shown in Figures 53-56.



Figure 53: von Mises stress (MPa) plot for a fillet radius of 4mm



Figure 54: Normal axial stress (MPa) plot for a fillet radius of 4mm

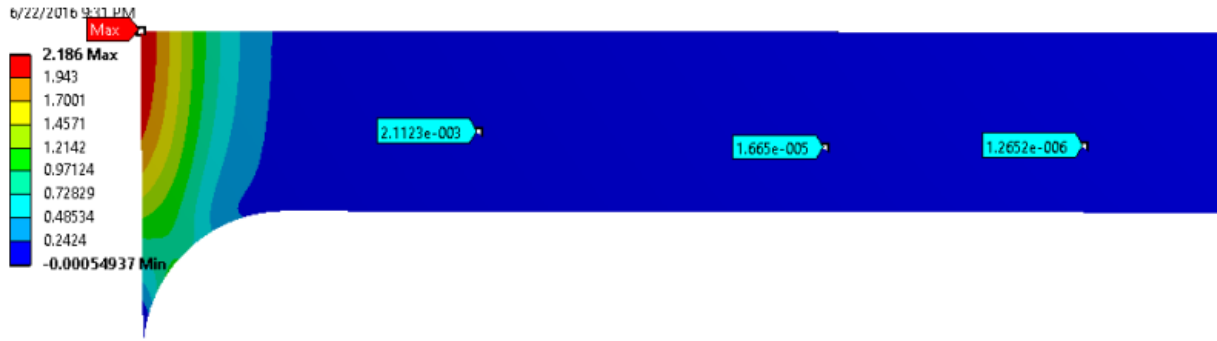


Figure 55: Normal radial stress (MPa) plot for a fillet radius of 4mm



Figure 56: Shear stress (MPa) plot for a fillet radius of 4mm

In Table 3, the maximum stress values along with the location of the maximum stress are shown for element size of 0.09. The results for element size 0.07 and 0.25 are shown in Appendix B-b.

Table 3: Maximum stress values and location for case III mesh size h sixe 0.09

<u>Radius (mm)</u>	<u>No of nodes</u>	<u>No of elements</u>	<u>Maximum displacement (mm)</u>	<u>Max equivalent stress (MPa) / Location</u>	<u>Shear stress (MPa) / Location</u>	<u>Normal stress (MPa) / Axial direction / Location</u>	<u>Normal stress (MPa) / Radial direction / Location</u>
1	53781	17680	3.827	5.396/ middle of the circle	0.0527 /at transition	4.322 / middle of the circle	3.125/ middle of the circle
2	54494	17911	3.809	3.308/ at the transition	0.0209 /at transition	3.366/ at the transition	2.385/ at the corner
3	55128	18115	3.789	3.611/ at the transition	0.0060 /at transition	3.699/ at the transition	2.294/ at the corner
4	56023	18404	3.767	3.819/ at the transition	0.0017 /at transition	3.915/ at the transition	2.185/ at the corner
5	57115	18762	3.742	3.912/ at the transition	0.00034 /at transition	4.013/ at the transition	2.064/ at the corner

Mesh sensitivity studies were performed and Figures 57-60 show the effect of the different element sizes on the ligament stresses and displacement when the fillet radius is varied. There is no variation in the displacement when the mesh size is changed. Figures 57-60 shows that von Mises stress and normal stress values are increased if we decrease the element size from 0.09 to 0.07 and decreases if we increase the element size from 0.09 to 0.25 which shows that the stress is mesh dependent. The stress increases with the increase in fillet radius and also there is only a small variation in the stress values for different mesh sizes as the edge length increases so the mesh size is adequate for the analysis.

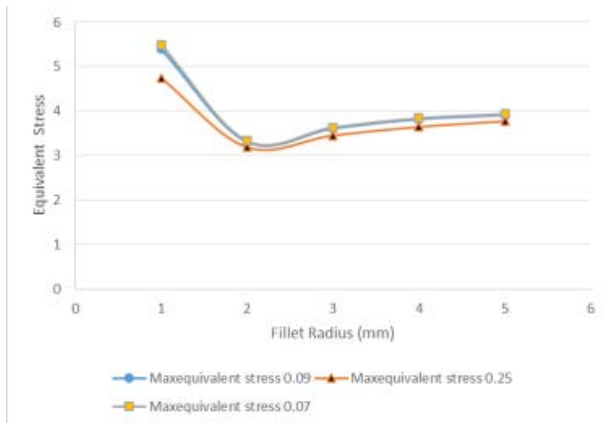


Figure 57: Mesh sensitivity for von Mises stress

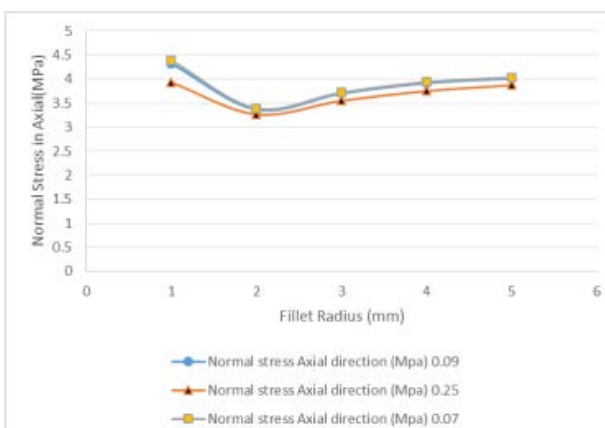


Figure 58: Mesh sensitivity for normal axial stress

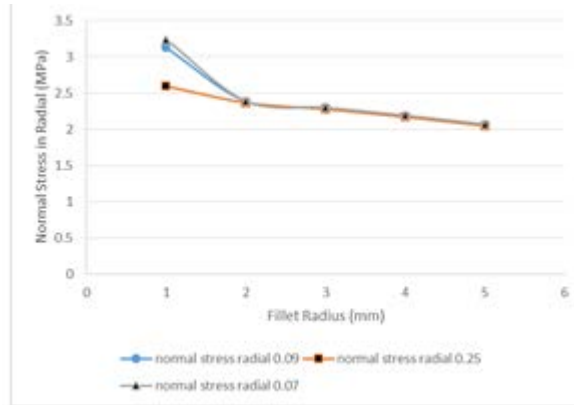


Figure 59: Mesh sensitivity for normal radial stress

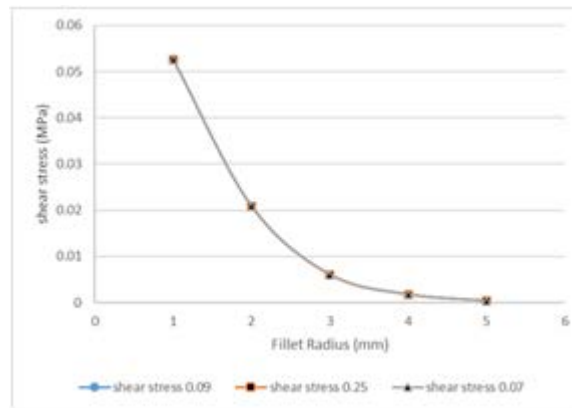


Figure 60: Mesh sensitivity for shear stress

7.4 EFFECT OF VARYING ANGLE

With this geometry, the angle of the ligament side was varied from 15 degrees to 75 degrees and four different cases were studied. Two sample cases are shown in Figures 61-62.



Figure 61: Case IV with angle 30 degrees



Figure 62: Case IV with angle 60 degrees

Figures 63-67 show the results of the finite element analysis for different angle for element size of 0.09. The values of the maximum equivalent stress, normal stress in axial and radial direction and end displacement is shown along with the number of nodes and elements used in the model. (Appendix B-c).

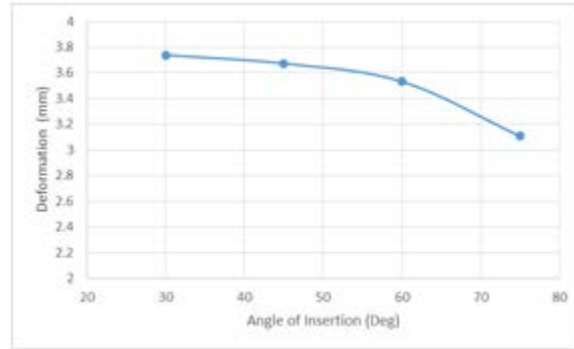


Figure 63: Maximum displacement vs angle

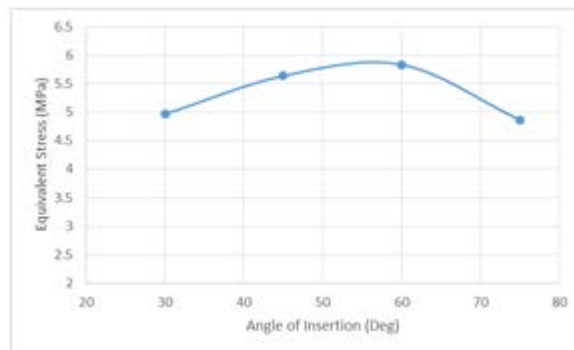


Figure 64: von Mises stress vs angle

Figures 65-66 shows the effect of the angle on the normal stress in radial and axial direction. The normal stress in axial direction increase when the angle is increased from 15 degrees to 60 degrees but decreases from 60 degrees to 75 degrees due to the higher stress concentration in the geometry due to the transition from angle to the straight line.

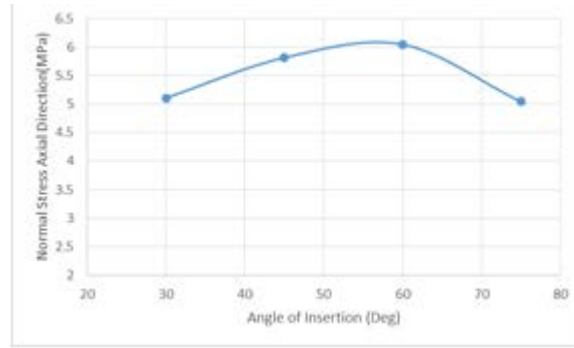


Figure 65: Normal axial stress vs angle

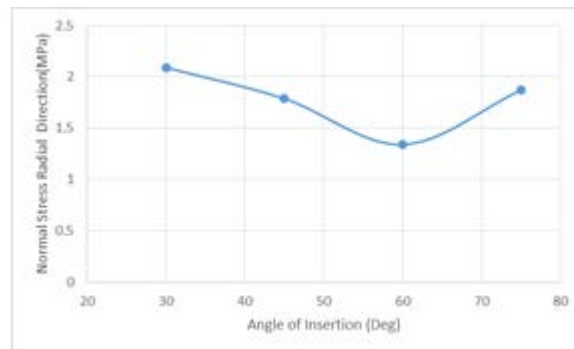


Figure 66: Normal radial stress vs angle

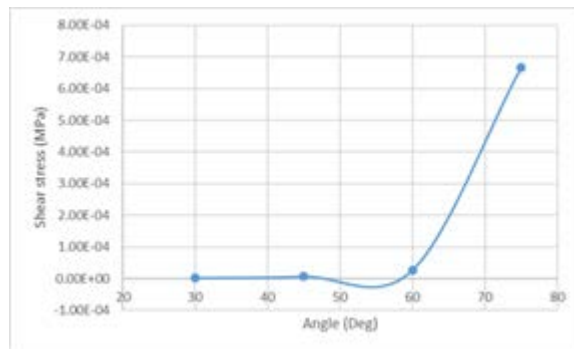


Figure 67: Shear stress vs angle

Plots of the distributions of the von Mises stress, normal axial stress, shear stress and normal radial stress for the fillet angle as 45 degrees are shown in Figures 68-71.

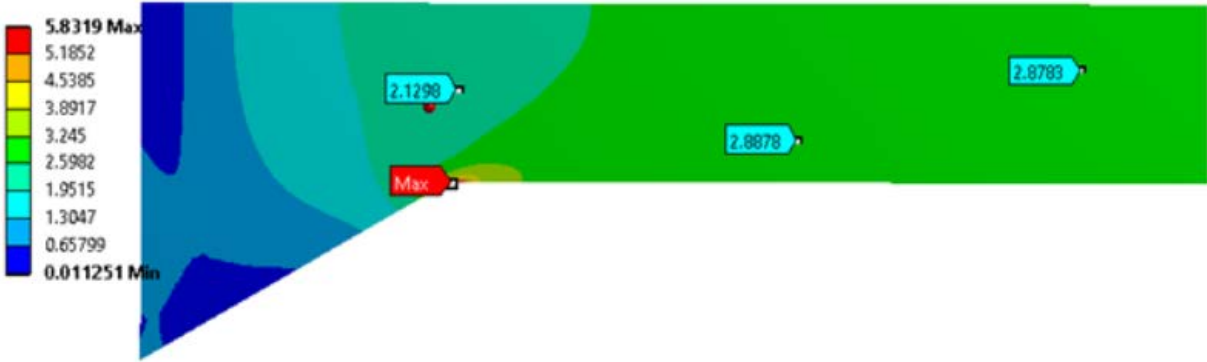


Figure 68: von Mises stress (MPa) plot for case IV (angle 45 deg.)

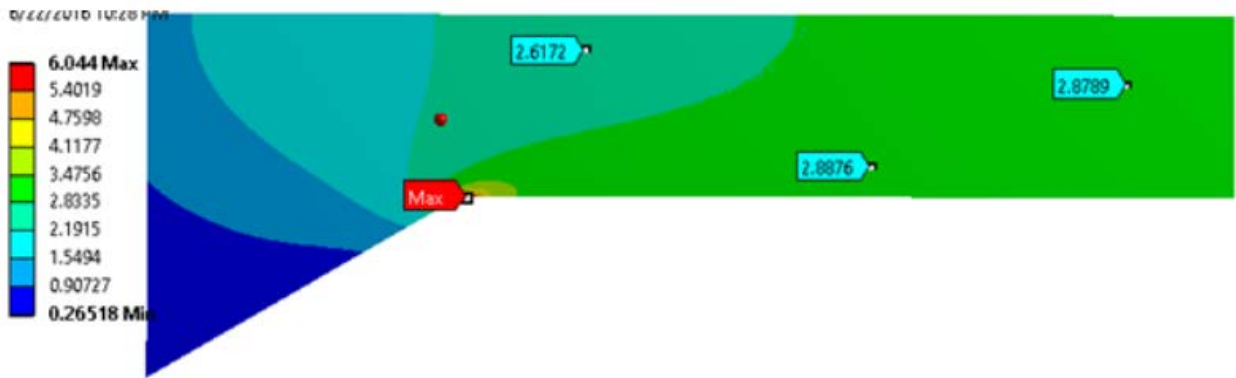


Figure 69: Normal radial stress (MPa) plot for case IV (angle 45 deg.)

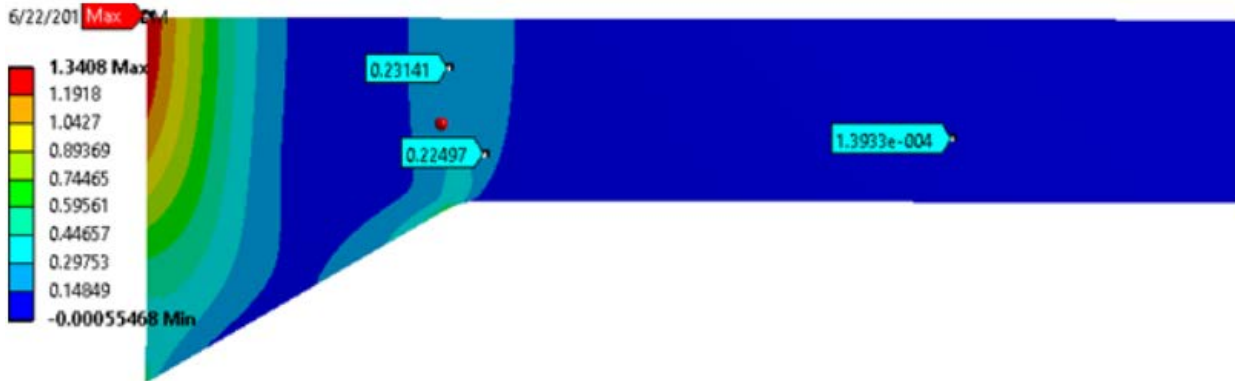


Figure 70: Normal radial stress (MPa) plot for case IV (angle 45 deg.)



Figure 71: Shear stress (MPa) plot for case IV (angle 45 deg.)

In Table 4, the maximum stress values along with the location of the maximum stress are shown for element size of 0.09. The results for element size 0.07 and 0.25 are shown in Appendix B-c.

Table 4: Maximum stress values and location for case IV (Element size 0.09)

Angle (deg)	No of nodes	No of elements	Maximum displacement (mm)	Max equivalent stress (MPa) / Location	Max Shear stress(MPa) /Location	Max Normal axial stress (MPa)/ Location	Max Normal radial stress(MPa) / Location
30	58400	19189	3.739	4.965/ at the transition	1.9150E-06/ at the tip	2.0905/ at the transition	5.108/at the center
45	60571	19912	3.673	5.634 /at the transition	6.6771E-06/ at the tip	1.7881/ at the transition	5.813/at the center
60	64285	21150	3.533	5.831 /at the transition	2.7464E-05 / at the tip	1.3408/ at the transition	6.044/at the center
75	73723	24298	3.107	4.863 /at the transition	6.679E-04 / at the tip	1.8702/ at the transition	5.041/at the center

Figures 72-75 shows the effect of the different mesh sizes on the finite element analysis was analyzed. Mesh sensitivity studies were performed. There is slight variation in the displacement when the mesh size is changed. Figure 72-75 shows the effect of different element sizes on the ligament stresses when the angle is varied. There is a small variation in the von Mises stress and normal axial and radial stress when the mesh size is varied from 0.07 to 0.25. As we increase the mesh size from 0.07 to 0.25 there is an increase in the values of equivalent

stress and normal stress. But then as the variation is less than 10% the mesh size of 0.09 is adequate for the analysis.

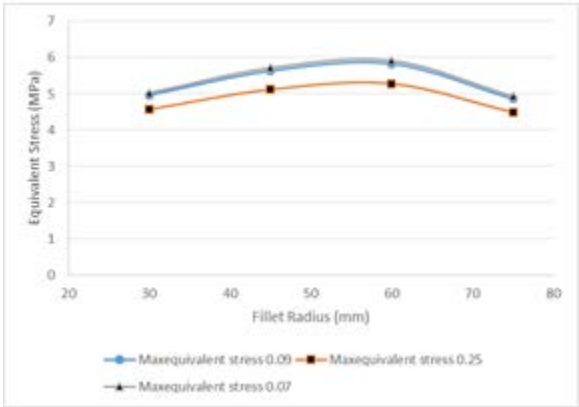


Figure 72: Mesh sensitivity for von Mises stress

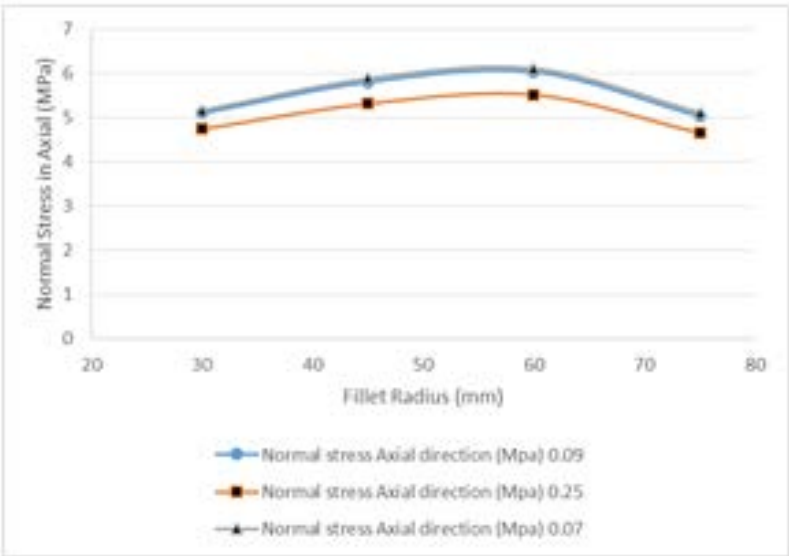


Figure 73: Mesh sensitivity for normal axial stress

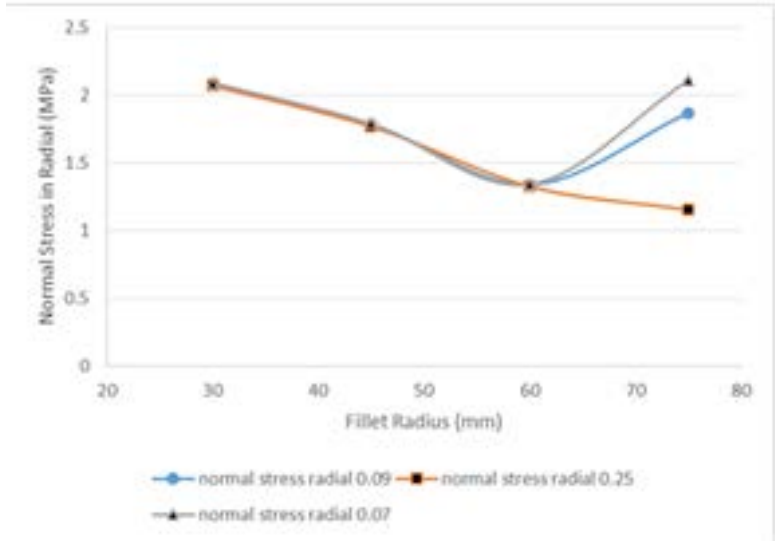


Figure 74: Mesh sensitivity for normal radial stress

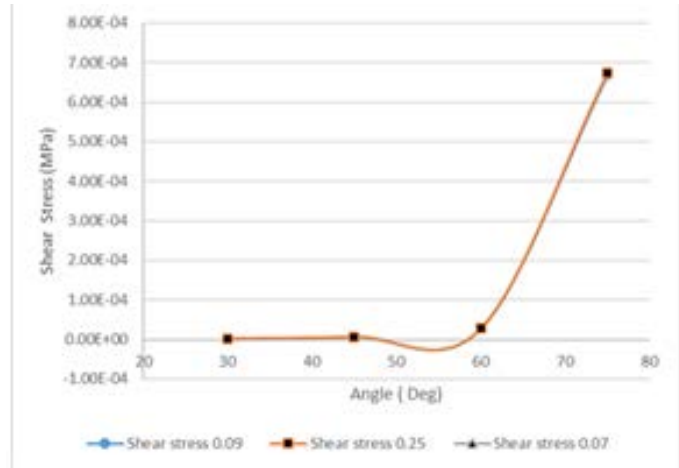


Figure 75: Mesh sensitivity for shear stress

7.5 EFFECT OF VARIABLE MINOR RADIUS

A elliptical shape was chose for the ligament attached with minor radius being varied from 6mm to 10mm in the increments of 1 mm and five different cases were studied. Two sample cases are shown below in Figures 76-77.



Figure 76: Case V with minor radius of 6mm



Figure 77: Case V with minor radius of 9mm

Figures 78-82 show the results of effect of the minor radius size on the displacement and maximum von Mises stress for mesh size of 0.09mm. With the increase in minor radius the displacement decreases but the equivalent stress and normal stress in axial direction increases. The values of the maximum equivalent stress, normal stress in axial and radial direction and

displacement is shown along with the number of nodes and elements used in model in Appendix B-d.

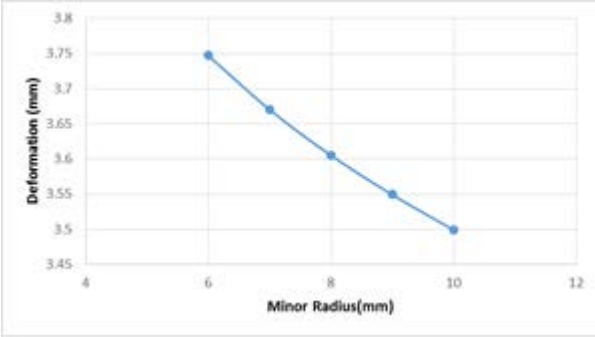


Figure 78: Displacement vs minor radius

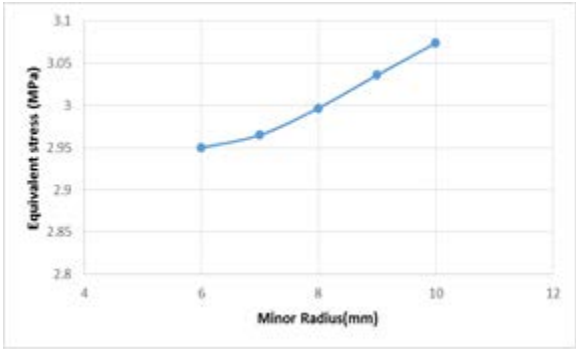


Figure 79: von Mises stress vs minor radius

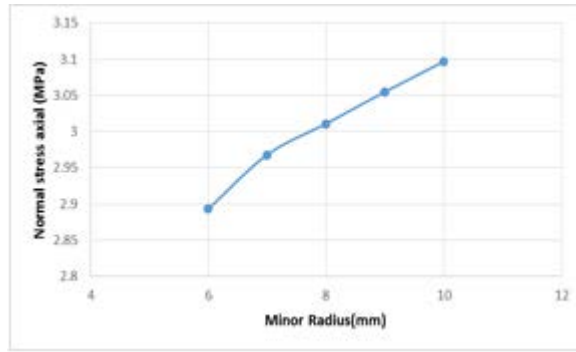


Figure 80: Normal axial stress vs minor radius

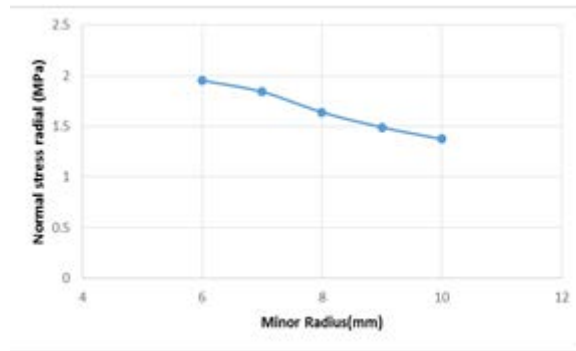


Figure 81: Normal radial stress vs minor radius

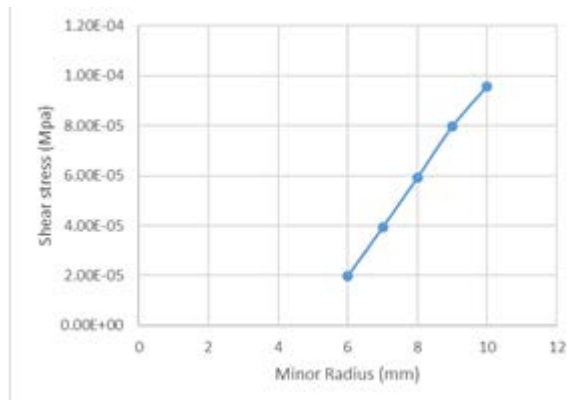


Figure 82: Shear stress vs minor radius

Plots of the distributions of the von Mises stress, normal axial stress, shear stress and normal radial stress for the minor radius of 8mm are shown in Figures 83-86.

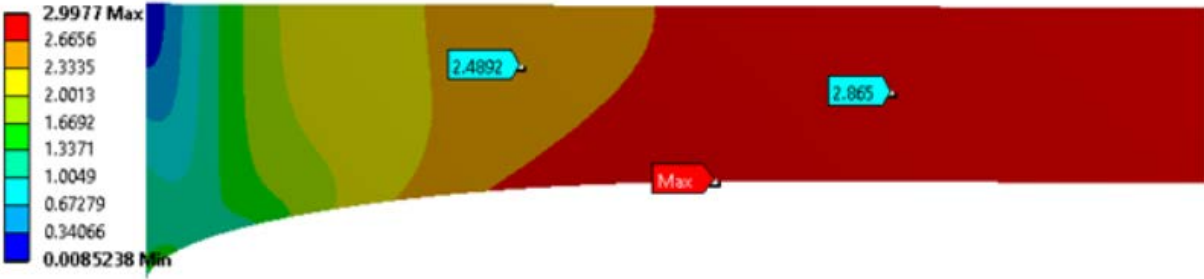


Figure 83: von Mises stress (MPa) plot for minor radius 8mm

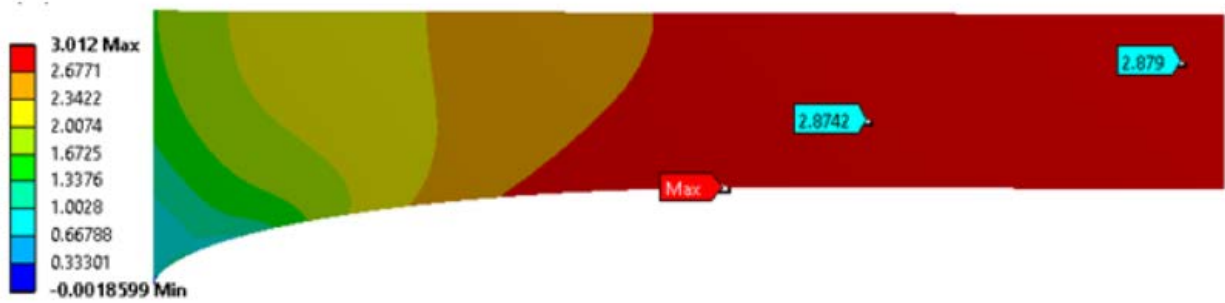


Figure 84: Normal axial stress (MPa) plot for minor radius 8mm



Figure 85: Normal radial stress (MPa) plot for minor radius 8mm



Figure 86: Shear stress (MPa) plot for minor radius 8mm

In Table 5, the maximum stress values along with the location of the maximum stress are shown for element size of 0.09. The results for element size 0.07 and 0.25 are shown in Appendix B-d.

Table 5: Maximum stress locations for case V (mesh size 0.09)

<u>Radius (mm)</u>	<u>No of nodes</u>	<u>No of elements</u>	<u>Maximum displacement (mm)</u>	<u>Max von Mises stress (MPa) / Location</u>	<u>Max Shear stress (MPa) / Location</u>	<u>Max Normal axial stress (MPa) / Location</u>	<u>Max Normal radial stress(MPa) / Location</u>
6	55797	18352	3.747	2.95/ at the corner	0.131/ at the corner	2.893/ at the corner	1.954 / at the center
7	57175	18808	3.670	2.965 / at the transition	0.08431/ at the corner	2.968/ at the transition	1.842/ at center
8	58547	19258	3.605	2.997/ at the transition	0.00715/ at the corner	3.011/ at the transition	1.640/ at center
9	60070	19759	3.549	3.036/ at the transition	0.00202/ at the corner	3.055/ at the transition	1.491/ at center
10	61657	20280	3.499	3.074/ at the transition	0.000246/ at the corner	3.097/ at the transition	1.375/ at center

Figures 87-90 shows the effect of the different element sizes on the finite element analysis was analyzed. There is no change in the displacement when we increase or decrease the mesh size. In Figures 87-90 equivalent stress and normal stress values are increased if we decrease the element

size from 0.09 to 0.07 and decreases if we increase the element size from 0.09 to 0.25 which shows that the stress is mesh dependent. Then as the variation is less than 10% the mesh size of 0.09 is adequate for the analysis.

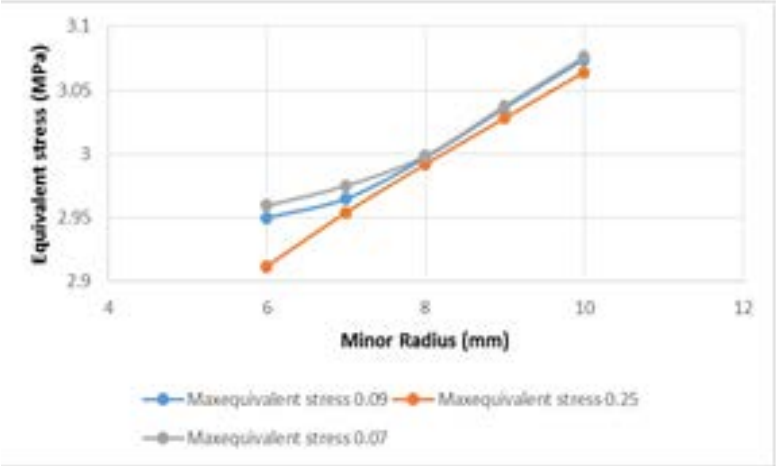


Figure 87: Mesh sensitivity for von Mises stress

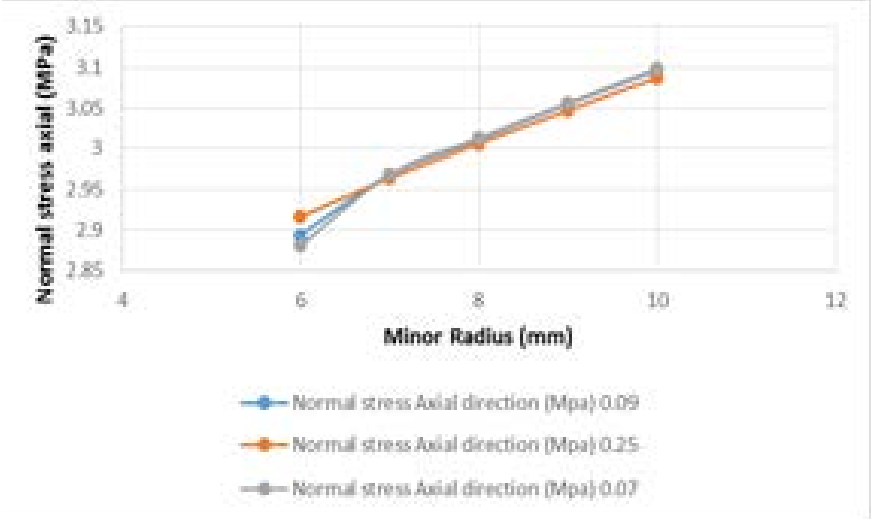


Figure 88: Mesh sensitivity for normal axial stress

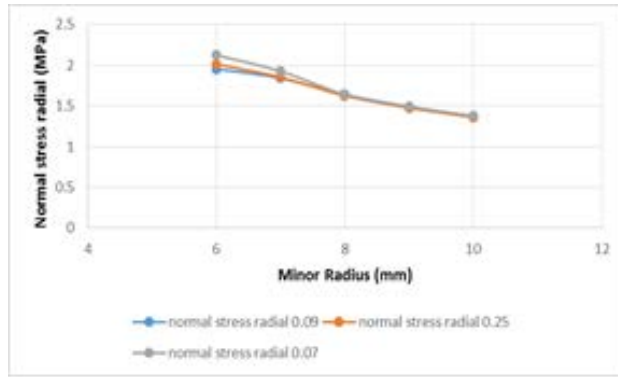


Figure 89: Mesh sensitivity for normal radial stress

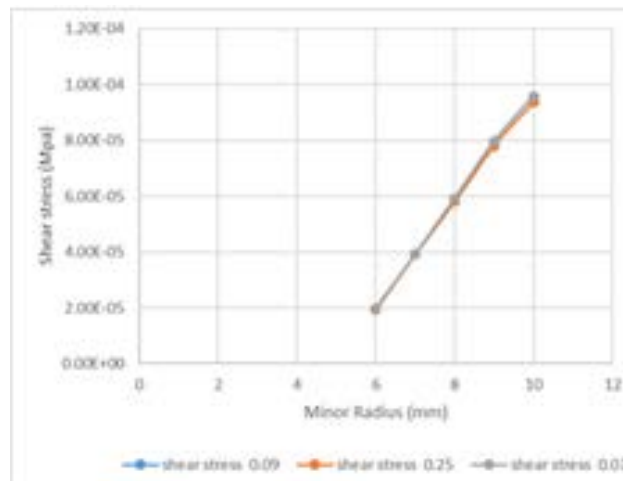


Figure 90: Mesh sensitivity for shear stress

7.6 DISCUSSION

From the results, we can note that stresses increase as the element size decreases from 0.25 to 0.09 to 0.07. The maximum increase in the von Mises stress with the change in element size from 0.09 to 0.07 is maximum in case 1 and case II out of all the cases. The element size has little or small effect on the displacement values for all the geometry cases. As the mesh becomes finer, the stresses are more accurate but also the computational time increases significantly. So

an optimum element size of 0.09 is suitable to get the results as the difference between the stress values for multiple mesh size is less than 10%.

The Piolletti's material model which was used to generate the material properties of the ligament is adequate for modeling the ligament because all the strain values calculated in the ligament model for different cases are less than 0.156 (Appendix A). The geometry of the ligament that has the maximum strain value is with the diameter of 10mm in case I, which has a strain of 0.159 and the maximum error between the Piolletti's model and the polynomial model is only 9.9%.

For the geometry with variable cylinder diameter, the maximum stress occurs at the corners of the cylinder. The maximum stress values decreases as we increase the diameter. The displacement of the ligament geometry also decreases as we increase the diameter. This geometry has the highest von Mises stress among all the geometries. The variable cylinder diameter has the highest effect on the von Mises stress, as we increase the cylinder diameter from 10mm to 20mm the stress is reduced by 80%.

For the tapered cylinder geometry, the maximum stress values occur at the corners of the cylinder where it attaches to the rigid bone. The maximum von Mises stress, normal axial and radial stress decreases as we increase the edge length. The displacement of the ligament geometry also decreases as we increase the edge length. There was a decrease of 74% in the maximum von Mises stress as we increased the edge length from 5mm to 10 mm, whereas the normal axial and radial stress were reduced by approximately 75% and 79%. The shear stress was reduced by 78%.

For the variable fillet radius geometry, the maximum stress values are located at the transition where the fillet radius changes into the straight section. In addition, when the fillet

radius is 1mm, the maximum stress values are at the middle of the arc and due to the mesh size and geometry there are high stress concentrations. When the fillet radius is increased from 2mm to 5 mm, the stress values increases and the maximum location is at the transition area. The displacement decreases as we increase the fillet radius. The normal stress in radial direction decreases when the fillet radius is increased from 1mm to 5mm. The difference in the von Mises stress as we increase the fillet radius from 1 mm to 5mm is decreased by 27.7% whereas the normal axial and radial stress is decreased by 30% approximately.

For the geometry with variable angle the maximum equivalent stress values occurs at the transition where the angle transitions into the straight line. As the angle increases the equivalent stress increases the equivalent stress increases until 60 degrees but then decreases from 60 degrees to 75 degrees and the maximum stress is at the transition area from the angle to the straight line.

For the geometry with variable radius of ellipse, the maximum stress values are the transition where the ellipse transitions into the straight section. All the geometric parameters studied in this analysis have an impact on the stresses of the ligament. The maximum von Mises stress values is when the radius of the ellipse is 6mm. The von Mises stress decreases as we increase the radius of the ellipse. The normal radial and axial stress also decreases as we increase the radius of the ellipse. The difference in the ligament stresses when the radius is increased from 6mm to 10mm is only 4.8%. This shows that the minor radius has the least effect on the stresses.

The simple cylinder shape of the ligaments has the highest von Mises stress among all the ligament geometry models as the difference between the maximum von Mises stress is around 80% when the edge length is increased from 5mm to 10 mm. The variable radius models have the least von Mises stress and as the difference between the stress values when we increase the

radius is only 4.8%, which shows that, the elliptical radius has the least effect on the ligament stress. The fillet angle and the minor radius do not have a major effect on the stresses.

Table 6 : Effect of geometry on von Mises stress for the same edge length

Edge length (mm)	Von Mises stress (Mpa)		
	tapered diameter	Fillet radius	variable minor radius
6	11.798	5.396	2.95
7	8.509	3.308	2.965
8	6.321	3.611	2.997
9	4.797	3.819	3.036
10	3.707	3.912	3.074

The tapered cylinder geometry has the highest von Mises stress for the same insertion site length among the fillet radius, variable minor radius. From Table 6, we notice that the minor radius with the 6mm edge length has the least von Mises stress. For higher insertion site length, there is a reduction in stresses across all the shapes.

8.0 CONCLUSION

From the results of the computational analysis in the present study, we can notice the importance of effect of shape of ligament on the stress at insertion sites. Also in the computational model, the mesh size significantly affects the stress in the ligament. The higher the mesh size more accurate the results and also more run time, the mesh size of 0.09 is suitable for meshing the ligament geometry because there is not much variation in the stress values if we used a mesh size lower than 0.09.

The Piolleti's material model, which was used for the material properties of the ligament is adequate for modeling the ligament because all the strain values calculated in the ligament model for different geometry cases are less than 0.156 for which the model is suitable.

The diameter, edge length and fillet radius have major effect on the stress on the ligament geometry. The stress values are more dependent on the angle in the ligament geometry, so more importance must be given to the cylinder diameter and fillet radius to evaluate the stresses in the ligament. The tapered cylinder geometry has the highest von Mises stress for the same insertion site length among the fillet radius, variable minor radius.

9.0 LIMITATIONS

There are some limitations in the current model, a 2D axis symmetry model was considered and also the bone was considered as rigid body. A more realistic approach would be to use a three dimensional model of ligament while also modeling the bone and modeling the contacts between the ligament and the bone which would give us better and accurate results. Also one could include the friction and calculate the contact stresses between ligament and bone that would help provide more insights into mechanics of human ligament. Also evaluating the fatigue analysis on ligament could provide much deeper insight into the mechanical properties of the ligament. Another limitation was the assumption of isotropy. In future work, one could model the ligament as a transversely isotropic composite like structure. To include anisotropy in the FE model, one could combine two separate strain energy functions for both the matrix and fiber. The matrix would be isotropic but the fibers would have a local material coordinate system applied to the long axis where directionally dependent material properties could be assigned.

APPENDIX A

MAXIMUM STRAIN VALUES CALCULATED

The strain values for the models are shown below for all the geometry cases. As we note that the strain values in all the geometries are less than 0.156, we can proceed using Pioletti material model to accurately model the ligament.

The maximum strain values for the variable cylinder diameter geometry case I are shown in Table 7.

Table 7 : Maximum strain values for case I (variable cylinder diameter)

Cylinder diameter	Maximum strain (mm/mm)
10	0.159
12	0.145
14	0.141
16	0.137
18	0.133
20	0.128

The maximum strain values for the variable edge length geometry case II are shown in Table 8.

Table 8: Maximum strain values for case II

Edge length	Maximum strain (mm/mm)
6	0.1587
7	0.1442
8	0.139
9	0.126
10	0.122

The maximum strain values for the variable fillet radius geometry case III are shown in Table 9.

Table 9: Maximum strain values for case III (fillet radius)

Fillet radius (mm)	Maximum strain (mm/mm)
1	0.1555
2	0.1502
3	0.1444
4	0.1373
5	0.1308

The maximum strain values for the variable fillet angle geometry case IV are shown in Table 10.

Table 10: Maximum strain values for case IV (fillet angle)

Fillet Angle (deg)	Maximum strain (mm/mm)
30	0.1468
45	0.1529
60	0.1545
75	0.1458

The maximum strain values for the variable elliptical minor radius geometry case V are shown in Table 11.

Table 11: Maximum strain values for case V (minor radius)

Minor Radius (mm)	Maximum strain (mm/mm)
6	0.1558
7	0.1469
8	0.13719
9	0.1249
10	0.1204

Based on the above strain values in Table 7-11, we could use the Piolleti's model for the ligament material model.

APPENDIX B

B.A: CASE II: EFFECT OF VARYING EDGE LENGTH

Below in the table the results of the stress and displacement along with the location of the maximum stresses along with the number of nodes and elements in the model are shown for the mesh density of 0.09. The results for the 3 different mesh sizes are also shown in the below table

Mesh Size 0.07

Table 12: Results for the case II with mesh size 0.07

<u>Edge (mm)</u>	<u>No of nodes</u>	<u>No of elements</u>	<u>Maximum displacement (mm)</u>	<u>Max equivalent stress (MPa) / Location</u>	<u>Shear stress (MPa) / Location</u>	<u>Normal stress (MPa) / Axial direction/ Location</u>	<u>Normal stress (MPa) / Radial direction/ Location</u>
10	85877	28318	3.8414	19.717/ Corner	11.060/ Corner	15.8096/ Corner	12.441/ Corner
12	95523	31528	3.514	13.719 / Corner	7.6835/ Corner	11.2083/ Corner	8.5713/ Corner
14	105519	34860	3.251	9.864/ Corner	5.5211/ Corner	8.15805/ Corner	6.1425/ Corner
16	116872	38639	3.027	7.280/ Corner	4.0729/ Corner	6.05814/ Corner	4.5054/ Corner
18	127958	42335	2.835	5.506/ Corner	3.0806/ Corner	4.59830/ Corner	3.3926/ Corner
20	139538	46189	2.670	4.228/ Corner	2.3672/ Corner	3.52580/ Corner	2.5942/ Corner

Mesh Size 0.25

Table 13: Results for the case II with mesh size 0.25

<u>Edge (mm)</u>	<u>No of nodes</u>	<u>No of elements</u>	<u>Maximum deformation (mm)</u>	<u>Max equivalent stress (MPa) / Location</u>	<u>Shear stress (MPa) / Location</u>	<u>Normal stress (MPa) / Axial direction / Location</u>	<u>Normal stress (MPa) / Radial direction / Location</u>
10	11360	3673	3.841	10.399/Corner	5.791/Corner	8.564 / corner	6.312/Corner
12	12429	4030	3.514	7.307/Corner	4.061/Corner	6.166/ corner	4.434/Corner
14	13506	4387	3.251	5.348/Corner	2.968/Corner	4.586 /corner	3.248/Corner
16	14714	4789	3.027	4.038/Corner	2.240/Corner	3.493 /corner	2.450/Corner
18	15813	5152	2.835	3.118/Corner	1.730/Corner	2.863/corner	1.890/Corner
20	17200	5613	2.670	2.671/Corner	1.364/Corner	2.860 /corner	1.489/Corner

The contour plots for displacement , maximum equivalent stress , normal stress in axial and radial direction for the three mesh densities are shown in the below figures when the edge length is 7mm .

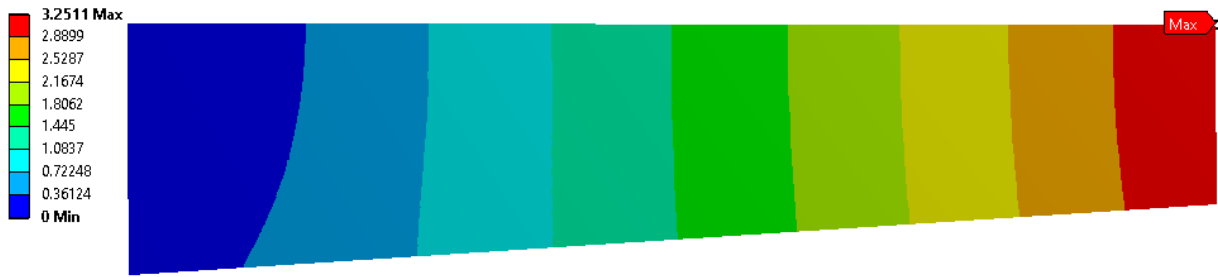


Figure 91: Displacement (mm) plot for mesh size 0.09

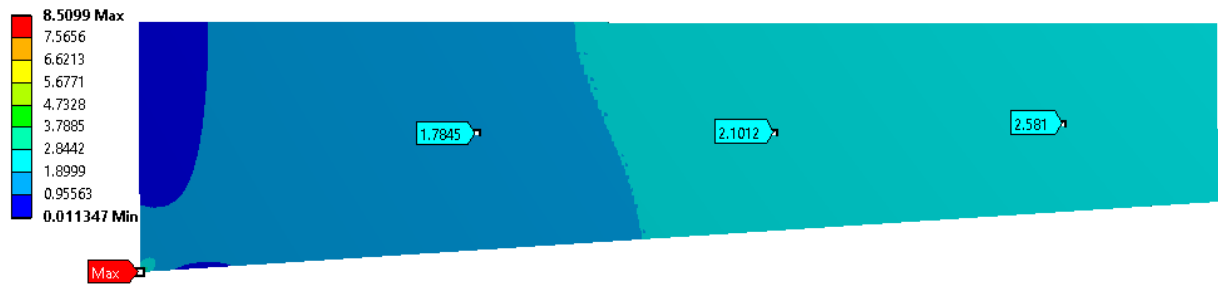


Figure 92: Equivalent stress (MPa) plot for mesh size 0.09

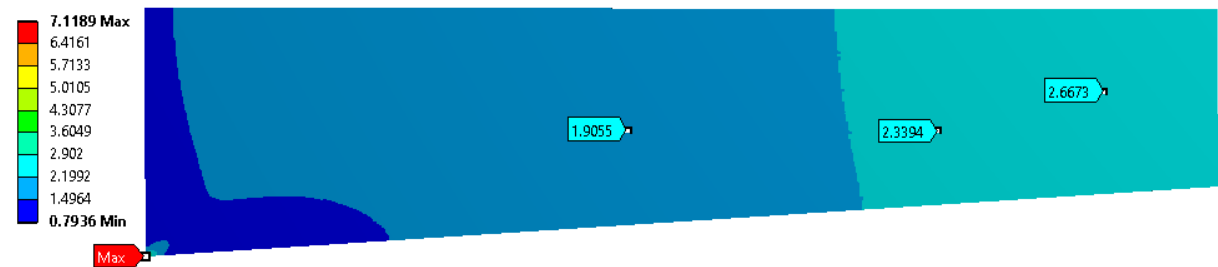


Figure 93: Normal axial stress (MPa) plot for mesh size 0.09

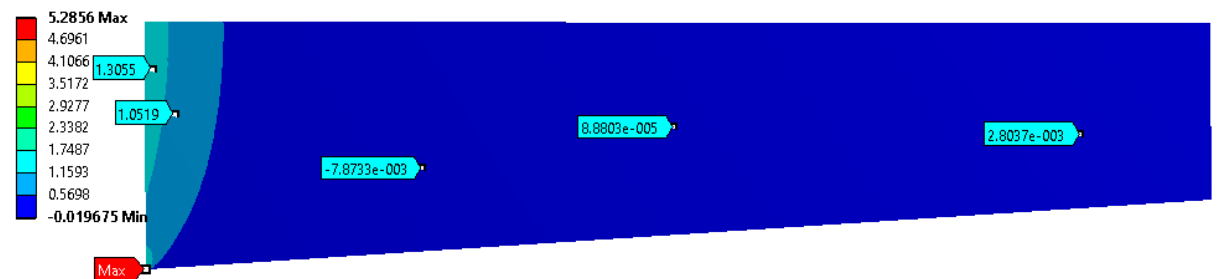


Figure 94: Normal radial stress (MPa) plot for mesh size 0.09

Mesh size : 0.07

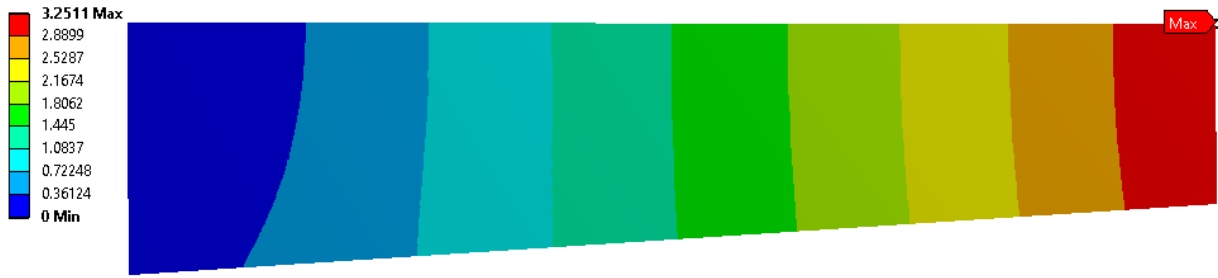


Figure 95: Displacement (mm) plot for mesh size 0.07

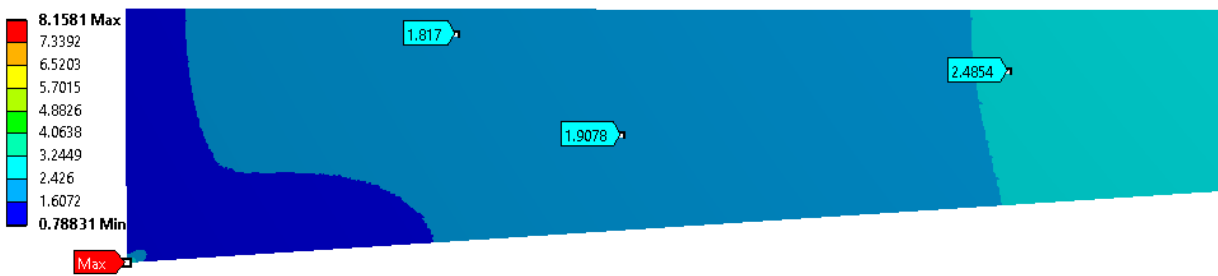


Figure 96: Normal axial stress (MPa) plot for mesh size 0.07

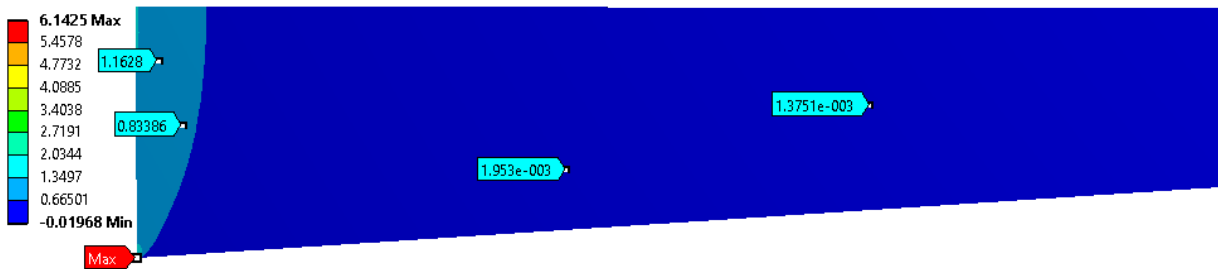


Figure 97: Normal radial stress (MPa) plot for mesh size 0.07

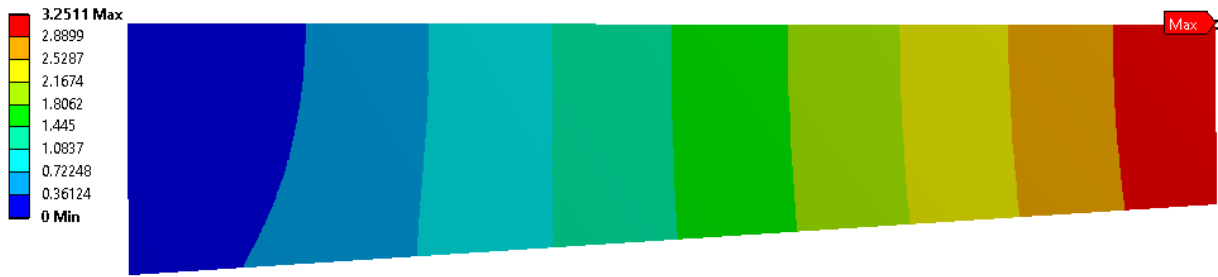


Figure 98: Displacement (mm) for mesh size 0.25



Figure 99: Equivalent stress (MPa) plot for mesh size 0.25

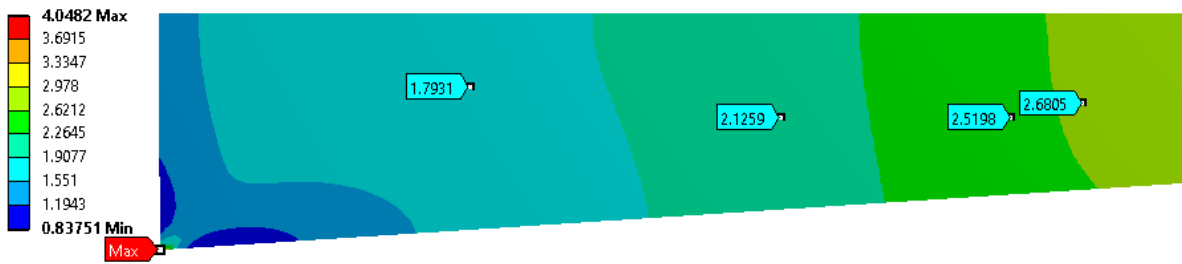


Figure 100: Normal axial stress (MPa) plot for mesh size 0.25

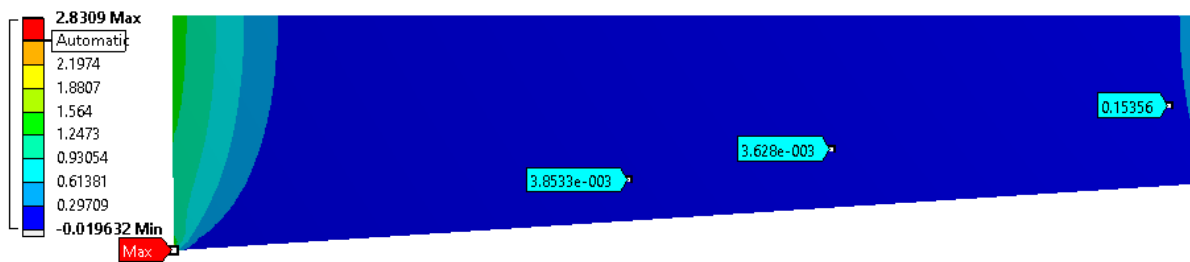


Figure 101: Normal radial stress (MPa) plot for mesh size 0.25

B.B: CASE III: EFFECT OF VARYING FILLET RADIUS

Below in the table the results of the stress and displacement along with the location of the maximum stresses along with the no of nodes and elements in the model are shown for the mesh density of 0.09. The results for the 3 different mesh sizes are also shown in the below table

Table 14: Results for the case III with mesh size 0.07

<u>Radius (mm)</u>	<u>No of nodes</u>	<u>No of elements</u>	<u>Maximum displacement (mm)</u>	<u>Max equivalent stress (MPa) / Location</u>	<u>Shear stress (MPa) / Location</u>	<u>Normal stress (MPa) / Axial direction/ Location</u>	<u>Normal stress (MPa) / Radial direction/ Location</u>
1	86529	28530	3.827	5.492 /at transition	0.0527 / at transition	4.3829 /at transition	3.2368 / at the corner
2	87625	28890	3.809	3.331/at transition	0.0209/ at transition	3.3922/at transition	2.3876/ at the corner
3	88819	29278	3.789	3.635/at transition	0.0060/ at transition	3.7205/at transition	2.2973/ at the corner
4	90599	29866	3.767	3.840/at transition	0.0017/ at transition	3.9371/at transition	2.1881/ at the corner
5	92815	30592	3.742	3.932 /at transition	0.000346/ at transition	4.0319/at transition	2.0669/ at the corner

Table 15: Results for the case III with mesh size 0.25

<u>Radius</u>	<u>No of nodes</u>	<u>No of elements</u>	<u>Maximum deformation (mm)</u>	<u>Max equivalent stress (MPa) / Location</u>	<u>Shear stress (MPa) / Location</u>	<u>Normal stress (MPa) / Axial direction / Location</u>	<u>Normal stress (MPa) / Radial direction / Location</u>
1	7265	2330	3.827	4.747/ at the transition	0.0525 /at transition	3.930/ at the transition	2.593/ middle of the circle
2	7371	2364	3.809	3.186/ at the transition	0.0208/at transition	3.265/ at the transition	2.365/ at the corner
3	7408	2375	3.789	3.453/ at the transition	0.0060/at transition	3.549/ at the transition	2.275/ at the corner
4	7438	2383	3.767	3.646/ at the transition	0.0017 /at transition	3.750/ at the transition	2.167/ at the corner
5	7557	2420	3.742	3.771/ at the transition	0.00034/at transition	3.871/ at the transition	2.046/ at the corner

The contour plots for displacement , maximum equivalent stress , normal stress in axial and radial direction for the three mesh densities are shown in the Figures 74-85 when the fillet radius is 4mm.



Figure 102 Displacement (mm) plot for mesh size 0.09

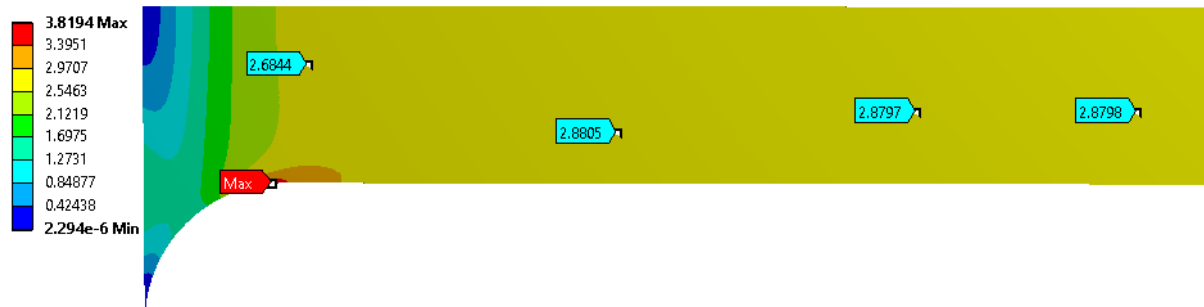


Figure 103: Equivalent stress (MPa) plot for mesh size 0.09



Figure 104: Normal axial stress (MPa) plot for mesh size 0.09



Figure 105: Normal radial stress (MPa) plot for mesh size 0.09



Figure 106: Displacement (mm) plot for mesh size 0.07



Figure 107: Equivalent stress (MPa) plot for mesh size 0.07

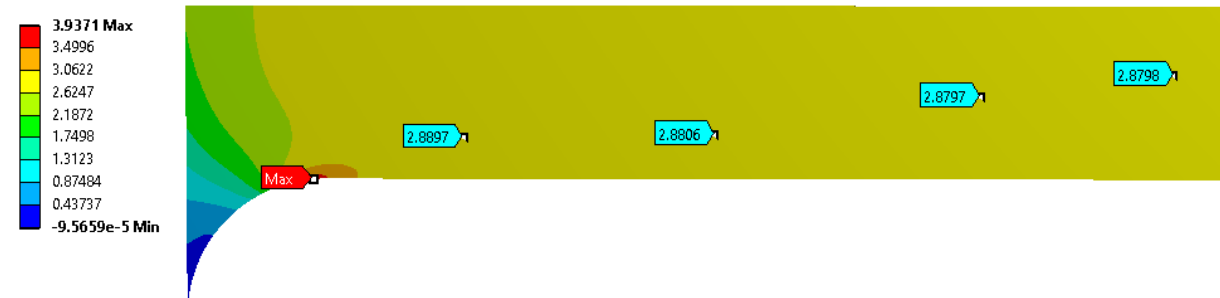


Figure 108: Normal axial stress (MPa) plot for mesh size 0.07



Figure 109: Normal radial stress (MPa) plot for mesh size 0.07

Mesh size : 0.25



Figure 110: Displacement (mm) plot for mesh size 0.25

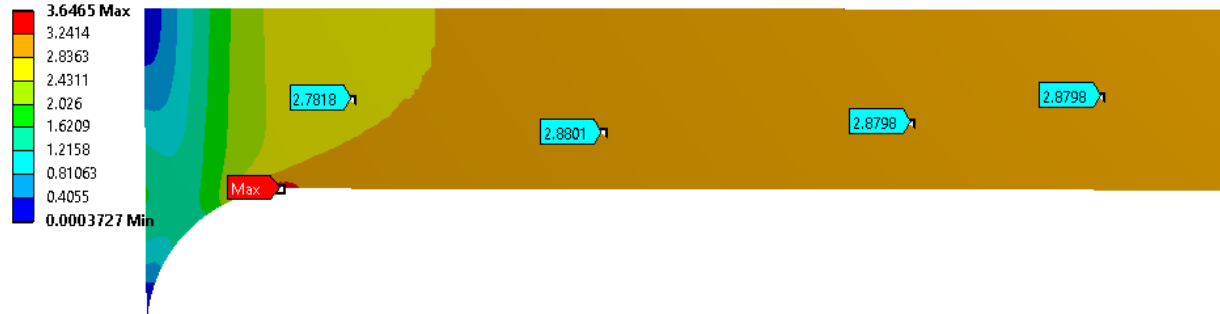


Figure 111: Equivalent stress (MPa) plot for mesh size 0.25



Figure 112: Normal axial stress (MPa) plot for mesh size 0.25

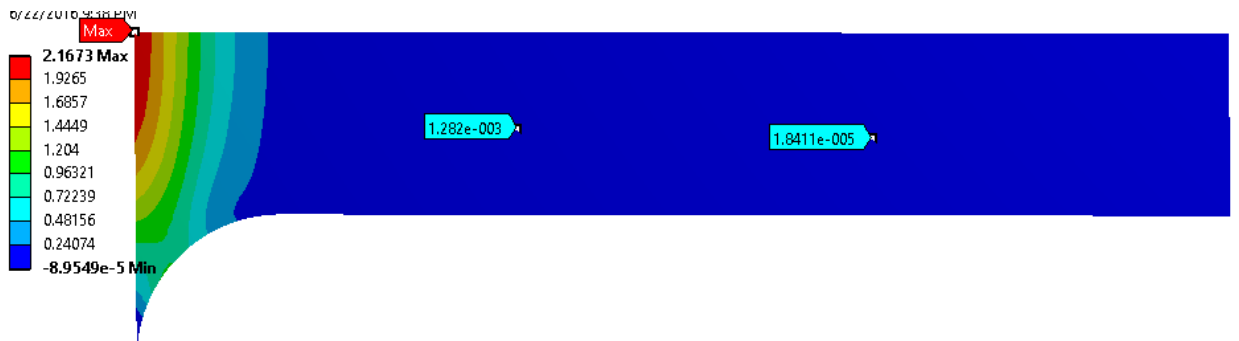


Figure 113: Normal radial stress (MPa) plot for mesh size 0.25

B.C: CASE IV: EFFECT OF VARYING ANGLE

In Table 9-10 the results of the stress and displacement along with the location of the maximum stresses along with the no of nodes and elements in the model are shown for the mesh density of 0.25 and 0.07. The results for the 3 different mesh sizes are also shown in the Table 9-10.

Table 16: Results for the case IV with mesh size 0.25

<u>Angle (deg)</u>	<u>No of nodes</u>	<u>No of elements</u>	<u>Maximum deformation (mm)</u>	<u>Max equivalent stress (MPa) / Location</u>	<u>Normal stress (MPa) / Axial direction/ Location</u>	<u>Normal stress (MPa) / Radial direction/ Location</u>
30	7735	2480	3.739	4.572/ at the transition	2.0717/ at the transition	4.7503/at the center
45	7961	2554	3.673	5.122 / at the transition	1.7704/ at the transition	5.3225/at the center
60	8454	2719	3.533	5.281 / at the transition	1.3271/ at the transition	5.5280/at the center
75	9575	3094	3.107	4.493 / at the transition	1.1538/ at the transition	4.6649/at the center

Table 17: Results for the case IV with mesh size 0.07

<u>Angle (deg)</u>	<u>No of nodes</u>	<u>No of elements</u>	<u>Maximum deformation (mm)</u>	<u>Max equivalent stress (MPa) / Location</u>	<u>Normal stress (MPa) / Axial direction/ Location</u>	<u>Normal stress (MPa) / Radial direction/ Location</u>
30	94900	31287	3.739	5.027/ at the transition	5.170/ at the transition	2.0928/at the center
45	98474	32477	3.673	5.717/ at the transition	5.892/ at the transition	1.7902/at the center
60	105170	34709	3.533	5.918/ at the transition	6.124/ at the transition	1.3423/at the center
75	120550	39841	3.107	4.934/ at the transition	5.126/ at the transition	2.1124/at the center

The contour plots for displacement , maximum equivalent stress , normal stress in axial and radial direction for the three mesh densities are shown in the Figures 86-97 for one iteration when the angle is 45 degrees.

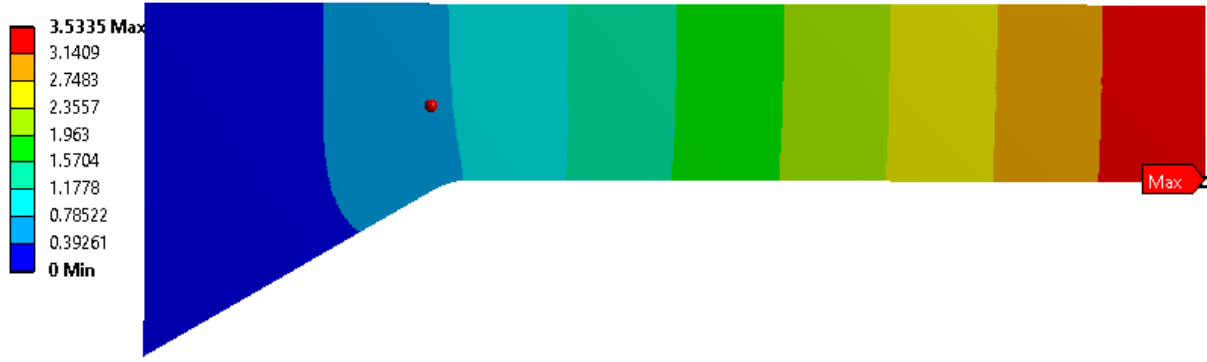


Figure 114: Displacement (mm) plot for mesh size 0.09

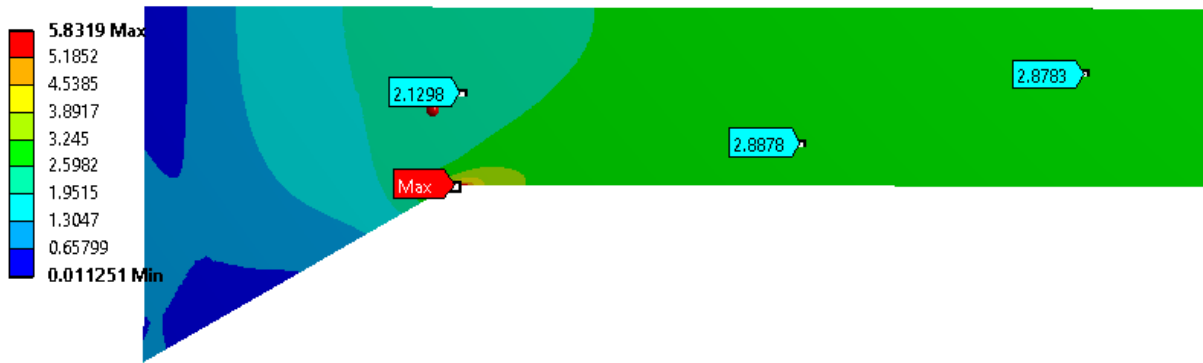


Figure 115: Equivalent stress (MPa) plot for mesh size 0.09

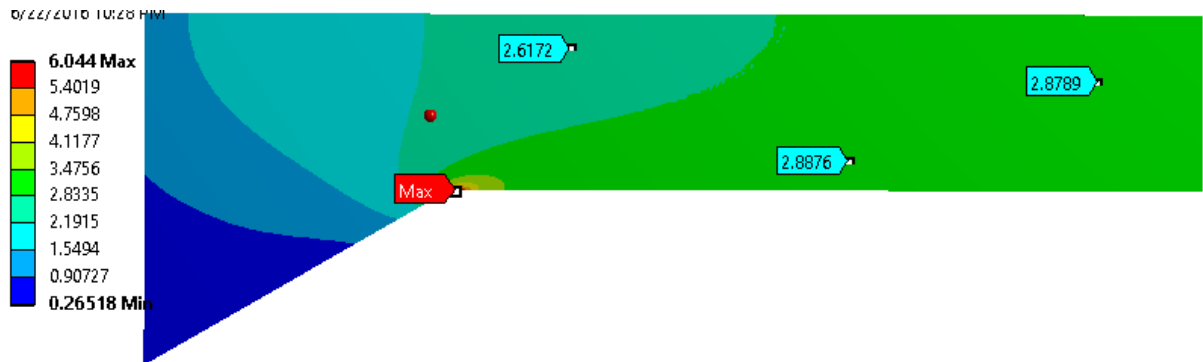


Figure 116: Normal axial stress (MPa) plot for mesh size 0.09

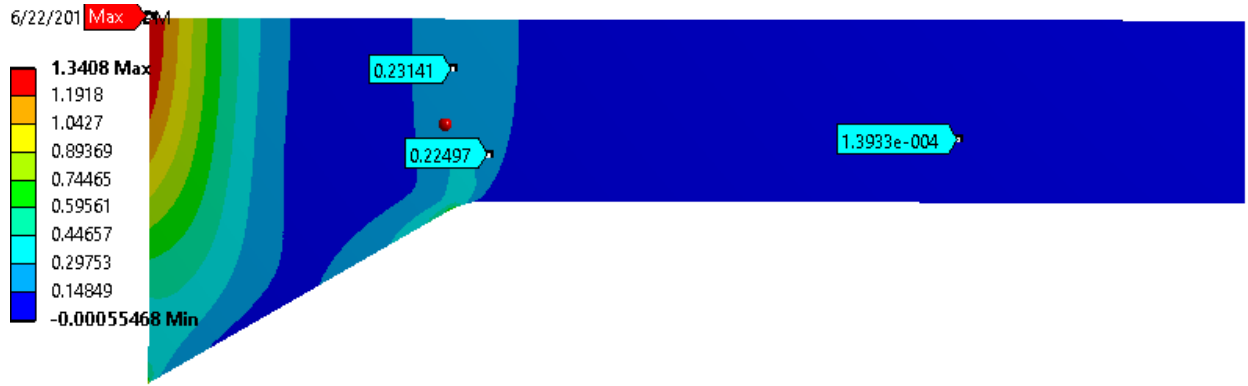


Figure 117: Normal radial stress (MPa) plot for mesh size 0.09

Mesh size : 0.25

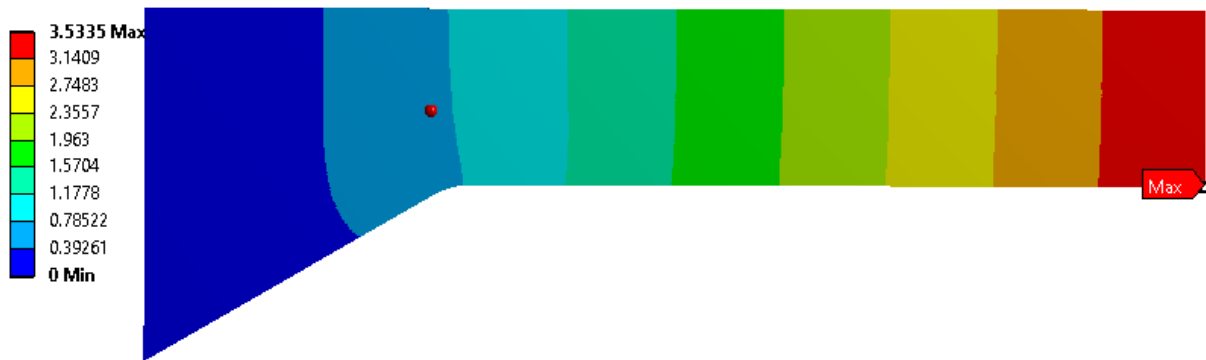


Figure 118: Displacement (mm) plot for mesh size 0.25

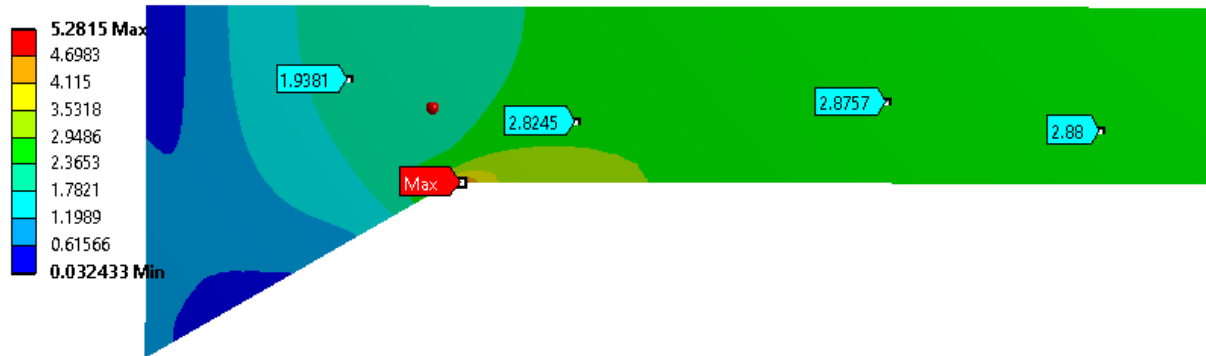


Figure 119: Equivalent stress (MPa) plot for mesh size 0.25

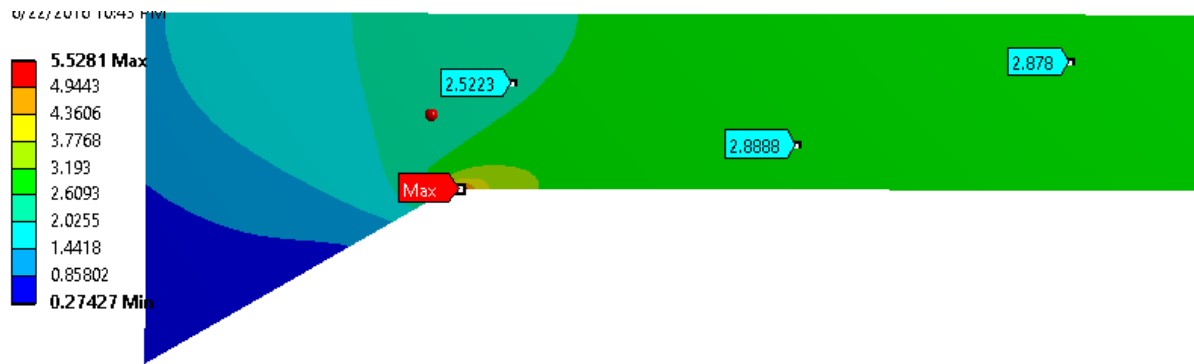


Figure 120: Normal axial stress (MPa) plot for mesh size 0.25

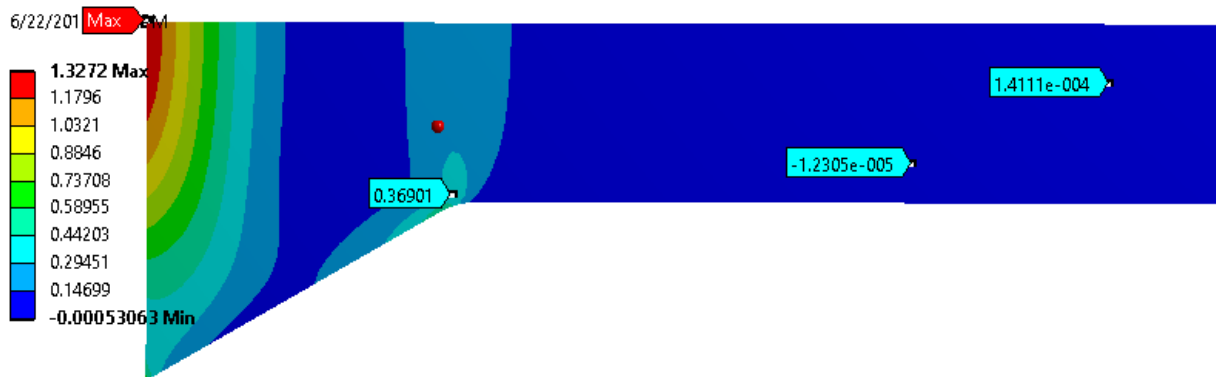


Figure 121: Normal radial stress (MPa) plot for mesh size 0.25

Mesh size 0.07



Figure 122: Displacement (mm) plot for mesh size 0.07

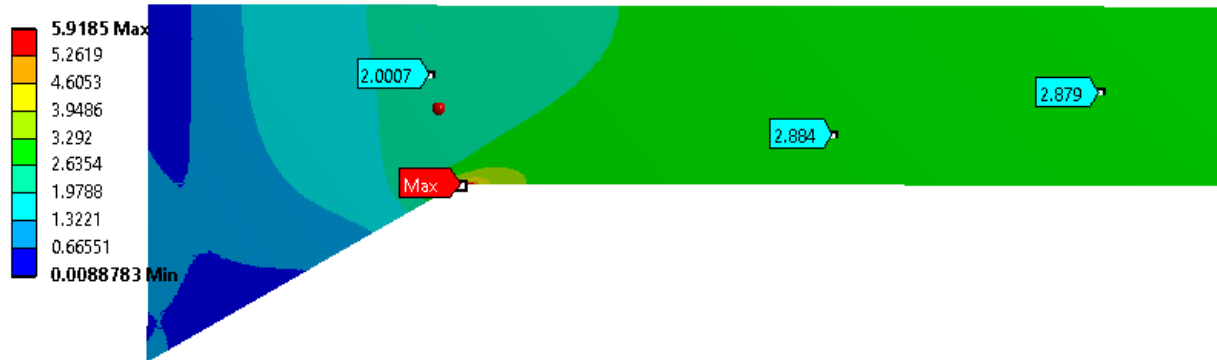


Figure 123: Equivalent stress (MPa) plot for mesh size 0.07

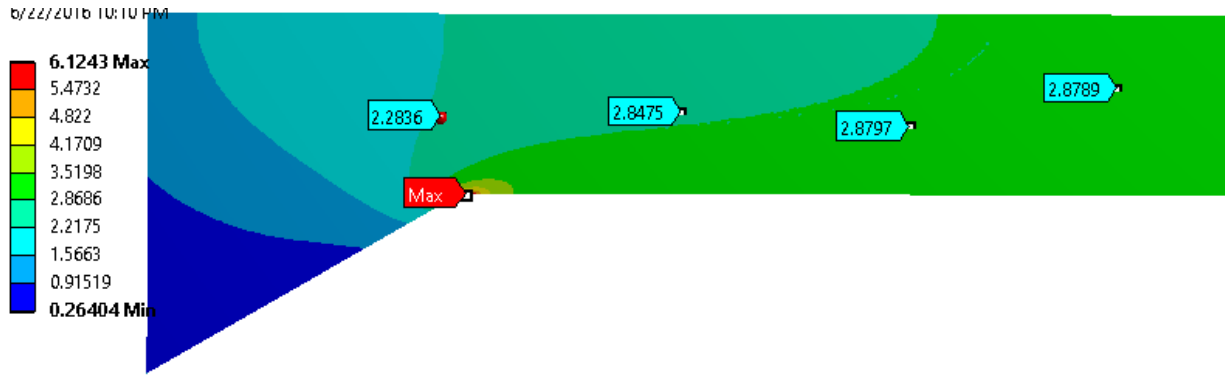


Figure 124: Normal radial stress (MPa) plot for mesh size 0.07

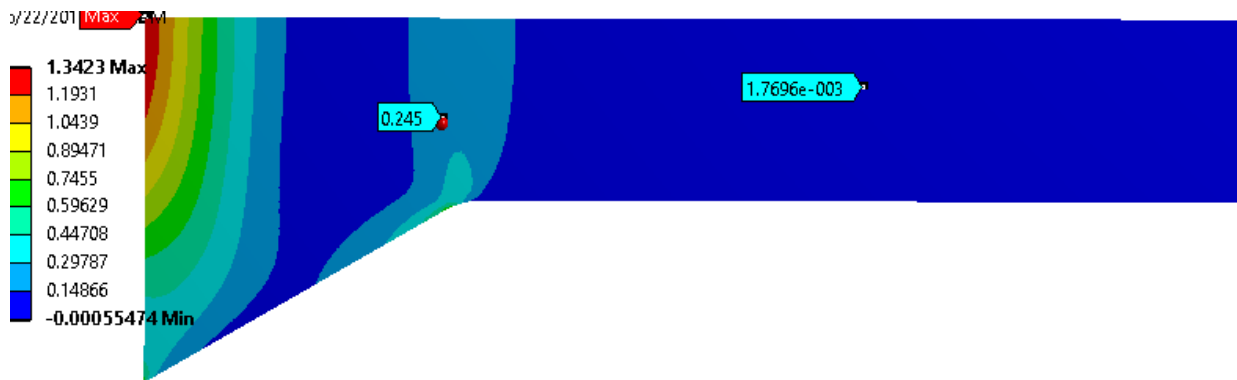


Figure 125: Normal radial stress (MPa) plot for mesh size 0.07

B.D: CASE V: EFFECT OF VARYING MINOR RADIUS

Below in the table the results of the stress and displacement along with the location of the maximum stresses along with the no of nodes and elements in the model are shown for the element size of 0.07 and 0.25.

Table 18: Results for the case V with mesh size 0.25

<u>Radius (mm)</u>	<u>No of nodes</u>	<u>No of elements</u>	<u>Maximum deformation (mm)</u>	<u>Max equivalent stress (MPa) / Location</u>	<u>Normal stress (MPa) / Axial direction/ Location</u>	<u>Normal stress (MPa) / Radial direction/ Location</u>
6	7418	2381	3.747	5.064/ at the transition	3.736/ at the transition	3.440/ at center
7	7563	2430	3.670	2.954/ at the transition	2.964/ at the transition	1.852/ at center
8	7816	2511	3.605	2.992/ at the transition	3.006/ at the transition	1.627/ at center
9	7941	2552	3.549	3.028/ at the transition	3.047/ at the transition	1.477/ at center
10	8099	2604	3.499	3.064/ at the transition	3.088/ at the transition	1.362/ at center

Table 19: Results for the case V with mesh size 0.07

<u>Radius (mm)</u>	<u>No of nodes</u>	<u>No of elements</u>	<u>Maximum deformation (mm)</u>	<u>Max equivalent stress (MPa) / Location</u>	<u>Normal stress (MPa) / Axial direction/ Location</u>	<u>Normal stress (MPa) / Radial direction/ Location</u>
6	89833	29634	3.747	6.79696 / at the transition	4.3171/ at the transition	4.9027/ at the center
7	92162	30405	3.670	3.05411/ at the transition	2.9684/ at the transition	1.9269/ at the center
8	94694	31241	3.605	2.99843/ at the transition	3.0126/ at the transition	1.6426/ at the center
9	97584	32197	3.549	3.03760/ at the transition	3.0563/ at the transition	1.4933/ at the center
10	100109	33028	3.075	3.07596/ at the transition	3.0990/ at the transition	1.3763/ at the center

The contour plots for displacement , maximum equivalent stress , normal stress in axial and radial direction for the three mesh densities are shown in the Figures 98-109 for one iteration when the angle is 45 degrees



Figure 126 : Displacement (mm) plot for mesh size 0.09

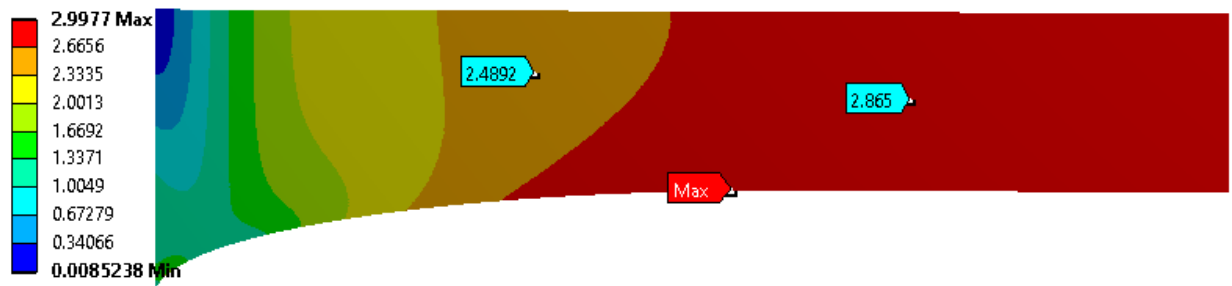


Figure 127: Equivalent stress (MPa) plot for mesh size 0.09

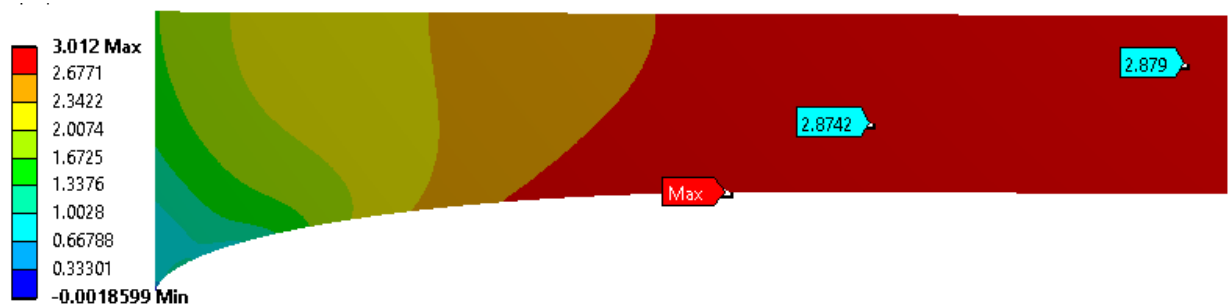


Figure 128: Normal axial stress (MPa) plot for mesh size 0.09



Figure 129: Normal radial stress (MPa) plot for mesh size 0.09

Mesh Size : 0.25

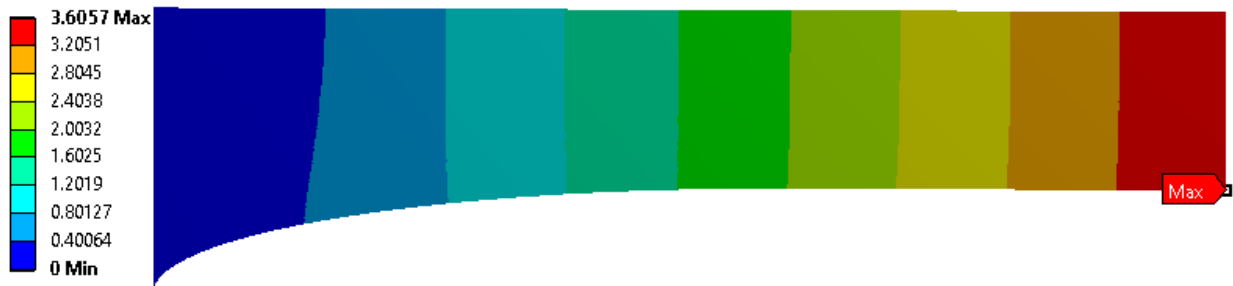


Figure 130: Displacement (mm) plot for mesh size 0.25

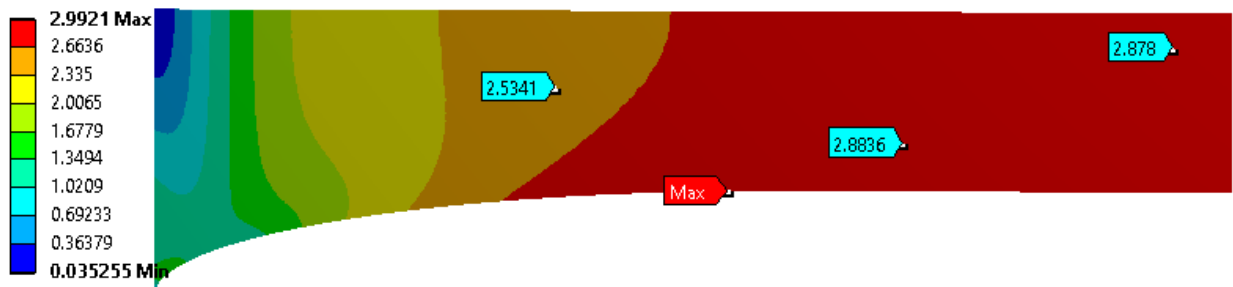


Figure 131: Equivalent stress (MPa) plot for mesh size 0.25

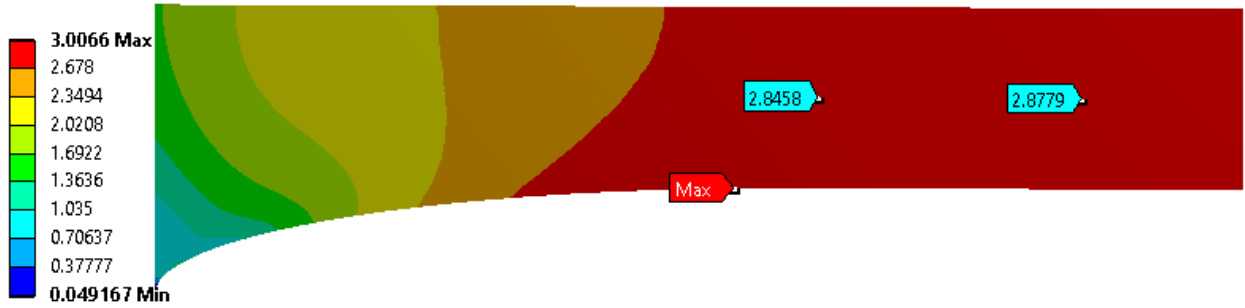


Figure 132: Normal axial stress (MPa) plot for mesh size 0.25

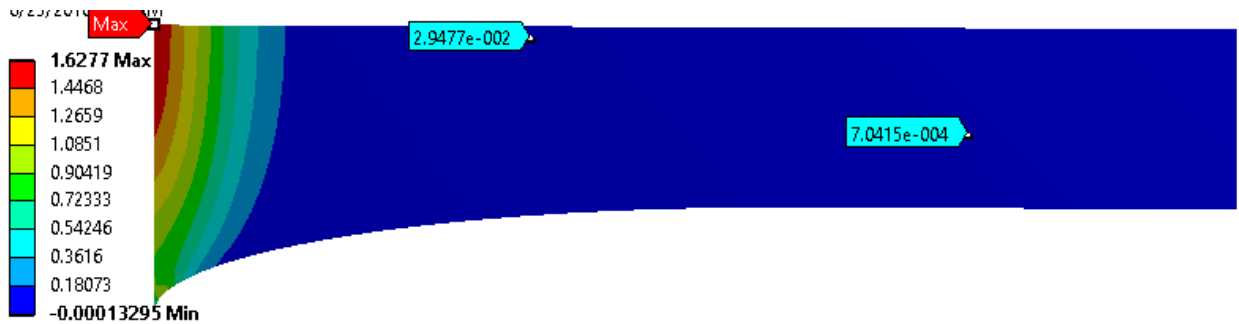


Figure 133: Normal radial stress (MPa) plot for mesh size 0.25

Mesh Size : 0.07

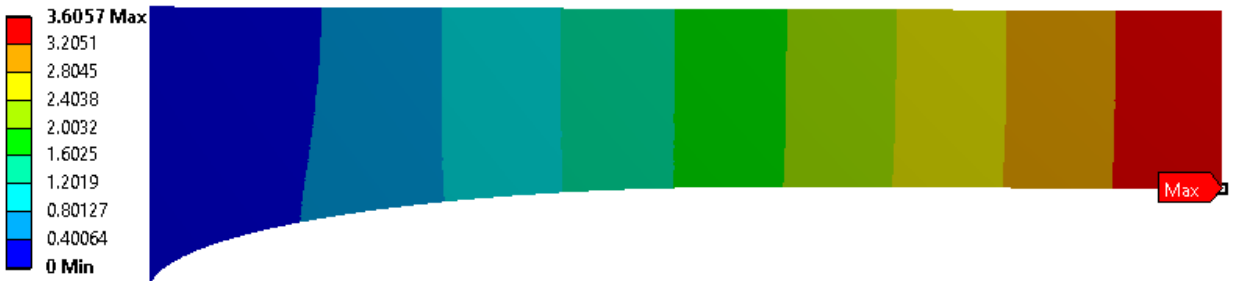


Figure 134: Displacement (mm) plot for mesh size 0.07

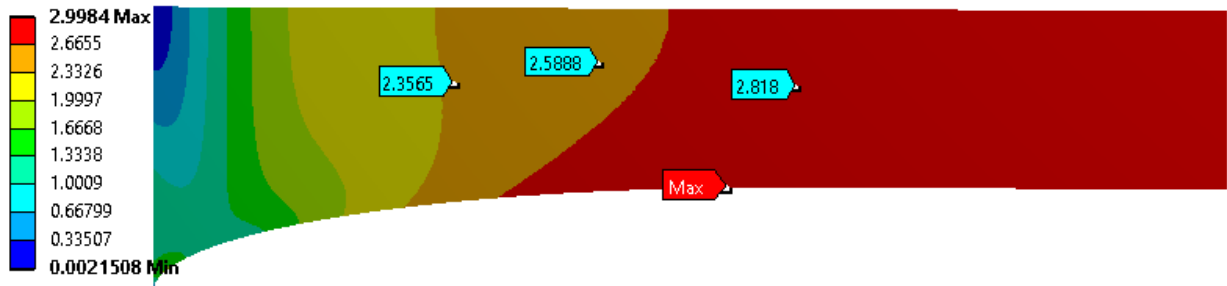


Figure 135: Equivalent stress (MPa) for mesh size 0.07

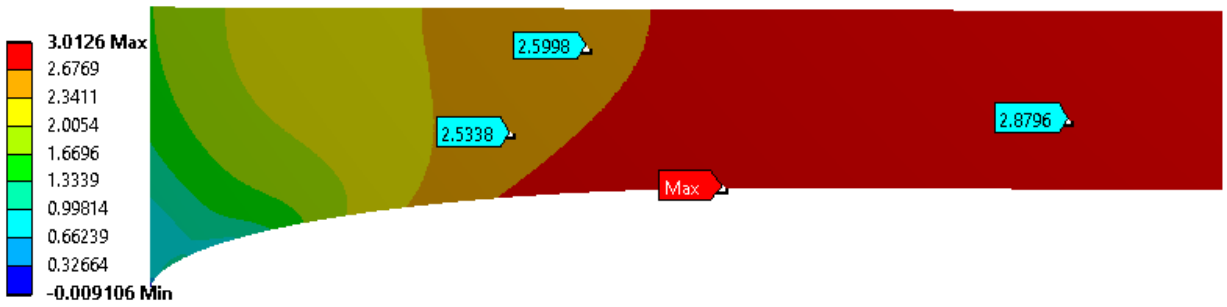


Figure 136: Normal axial stress (MPa) plot for mesh size 0.07

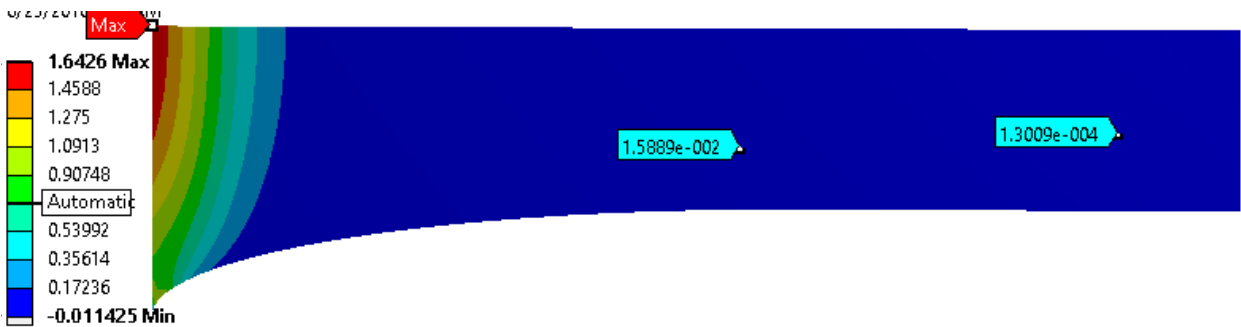


Figure 137: Normal radial stress (MPa) plot for mesh size 0.07

BIBLIOGRAPHY

- Ansys Inc. (n.d), 'ANSYS Mechanical User Manual'.
- Benjamin M. et al. . Where tendons and ligaments meet bone: attachment sites ('entheses') in relation to exercise and/or mechanical load. *J. Anat.* 208, 471–490 (2006).
- Crowninshield, R.D., Pope, M.H., 1976. The strength and failure characteristics of rat medial collateral ligaments. *J.Trauma* 16, 99-105.
- D.L. Butler, Y. Guan, M.D. Kay, J.F. Cummings, S.M. Feder, M.S. Levy Location-dependent variations in the material properties of the anterior cruciate ligament *Journal of Biomechanics*, 25 (1992), pp. 511–518
- Comninou M, Yannas IV. Dependence of Stress-Strain Non-linearity of Connective Tissue on the Geometry of Collagen Fibers. *Journal of Biomechanics*. 1976; vol. 9: 427-33
- Danto M, Woo SL. The Mechanical Properties of Skeletally Mature Rabbit Anterior Cruciate Ligament and Patellar Tendon Over a Range of Strain Rates. *Journal of Orthopaedic Research*. 1993 (11); 58-67
- Danyal H Nawabi, Scott Tucker , Kristofer J. Jones. "The Direct Insertion of the ACL Carries More Load than the Indirect Insertion: An Important Consideration When Performing Anatomic ACLR" *The Orthopaedic Journal of Sports Medicine*, 2(3)(suppl 1) DOI: 10.1177/2325967114S00008
- Debski, R.E., Song, Y., Musahl, V., Thomas, M., and Woo, S., 2004, "A Three Dimensional Finite Element Model of the Human Anterior Cruciate Ligament: A Computational Analysis with Experimental Validation," *Journal of Biomechanics*, pp. 383-390
- Duenwald S, Vanderby R, Lakes RS. Constitutive Equations for Ligament and Other Soft Tissue: Evaluation by Experiment. *Acta Mechanica*. 2009; 205: 23-33
- Freddie H Fu, Master technique in Orthopaedic surgery; Sports Medicine. 2008
- Holzapfel G A, Non-linear Solid Mechanics: A Continuum Approach for Engineering. John Wiley and Sons. 2000.

- Kelc Robi, Naranda Jakob, Kuhta Matevz and Vogrin Matjaz (2013). The Physiology of Sports Injuries and Repair Processes, Current Issues in Sports and Exercise Medicine, Associate Prof. Michael Hamlin (Ed.), InTech, DOI: 10.5772/54234
- Kevin D. Plancher, Robert K. Peterson, Jack C. Johnston, Timothy A. Luke. The Spino glenoid Ligament The Journal of Bone & Joint Surgery Feb 2005, 87 (2) 361-365; DOI: 10.2106/JBJS.C.01533
- Lu, Helen H., and Thomopoulos. "Functional attachment of soft tissues to bone: development, healing, and tissue engineering." Annual review of biomedical engineering 15 (2013): 201.
- Limbert G, Taylor M, Middleton J. Three Dimensional Finite Element Modeling of the Human ACL: Simulation of Passive Knee Flexion with a Stressed and Stress-free ACL. Journal of Biomechanics vol. 37 (2004) 1723-1731.
- Martin B, Burr D, Sharkey N. *Skeletal Tissue Mechanics*. Springer-Verlag. New York. 1998.
- Matyas, J.R., Anton, M.G., Shrive, N.G., Frank, C.B., 1995. Stress governs tissue phenotype at the femoral insertion of the rabbit MCL. Journal of Biomechanics 28, 147-157.
- M. Abramowitz & I. Stegun (1970): Handbook of mathematical functions. New York: Dover Publications.
- Michael Rackl. Curve Fitting for Ogden, Yeoh and Polynomial Models. 2015.
- M. B. Panzer and D. S. Cronin, "C4-C5 segment finite element model development, validation, and load-sharing investigation," J Biomech, vol. 42, pp. 480-90, Mar 11 2009
- Pena E. Calvo B. Martinez M. Doblare M. An Anisotropic Visco - hyper elastic Model for Ligaments at Finite Strains. Formulation and Computational Aspects. *International Journal of Solids and Structures*. 44. (2007). Pp 760-778.
- Pioletti, DP, Rakotomanana, LR, Benvenuti, JF, Leyvraz PF. Viscoelastic Constitutive Law in Large Deformations: Application to human knee ligaments and tendons. Journal of Biomechanics. 31 1998, 753-757.
- R. S. Rivlin and D. W. Saunders., Large Elastic Deformations of Isotropic Materials VII. Experiments on the Deformation Of Rubber, 1951, *Philosophical Transactions of the Royal Society of London, series A* , 243, 251-288.
- Song Y, Debski R, Musahl V, Thomas M, Woo S L-Y. A Three Dimensional Finite Element Model of the Human Anterior Cruciate Ligament: A Computational Analysis with Experimental Validation. *Journal of Biomechanics*. 37 (2004) 383-390.

- Speer KP, Warren RF, Wickiewicz TL, Horowitz L, Henderson L. Observations on the injury mechanism of anterior cruciate ligament tears in skiers. *Am J Sports Med.* 1995; 23: 77-81.
- Thomopoulos S, Marquez JP, Weinberger B, Birman V, Genin GM (2006) Collagen fiber orientation at the tendon to bone insertion and its influence on stress concentrations. *J Biomech* 39(10):1842–1851
- Veronda, D.R., Westmann, R.A., Mechanical Characterization of skin-finite deformations. *Journal of Biomechanics.* 3 (1970) 111-124.
- Mow VC et al (1991) Structure and function of articular cartilage and meniscus. In: Mow VC, Hayes WC (eds) *Basic orthopedic biomechanics.* Raven, New York
- Weiss J, Gardiner J. Computational Modeling of Ligament Mechanics. *Critical Reviews in Biomedical Engineering.* 29(4): 1-70. 2001.
- Weiss JA, Gardiner JC, Ellis BJ, Lujan TJ, Phatak NS. Three-dimensional Finite Element Modeling of Ligaments: Technical aspects. *Medical Engineering and Physics.* 27 (2005) 845-861.
- Zhang X, Guotai J, Wu C, Woo S. L-Y. A Subject Specific Finite Element Model of the Anterior Cruciate Ligament. *IEEE EMBS Conference Proceedings.* August 2008.